J. Fluid Mech. (2023), *vol*. 975, A32, doi:10.1017/jfm.2023.888

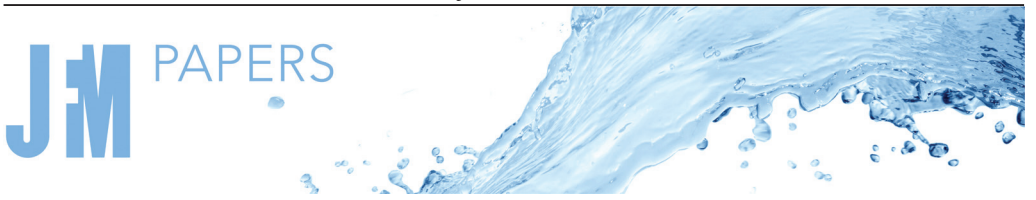

Dual scaling and the *n*-thirds law in grid turbulence

S.L. Tang[1],†, R.A. Antonia[2] and L. Djenidi[3,4]

[1]Center for Turbulence Control, Harbin Institute of Technology, Shenzhen 518055, PR China

[2]Discipline of Mechanical Engineering, College of Engineering, Science and Environment, University of Newcastle, Newcastle 2308, NSW, Australia

[3]Department of Mechanical Engineering, Indian Institute of Technology – Bombay, Powai, Mumbai 400076, India

[4]School of Electrical and Mechanical Engineering, Faculty of Sciences, Engineering and Technology, The University of Adelaide, Adelaide 5005, WA, Australia

(Received 26 December 2022; revised 2 September 2023; accepted 18 October 2023)

A dual scaling of the turbulent longitudinal velocity structure function $\overline{(\delta u)^n}$, i.e. a scaling based on the Kolmogorov scales (u_K, η) and another based on (u', L) representative of the large scale motion, is examined in the context of both the Kármán–Howarth equation and experimental grid turbulence data over a significant range of the Taylor microscale Reynolds number Re_λ. As Re_λ increases, the scaling based on (u', L) extends to increasingly smaller values of r/L while the scaling based on (u_K, η) extends to increasingly larger values of r/η. The implication is that both scalings should eventually overlap in the so-called inertial range as Re_λ continues to increase, thus leading to a power-law relation $\overline{(\delta u)^n} \sim r^{n/3}$ when the inertial range is rigorously established. The latter is likely to occur only when $Re_\lambda \to \infty$. The use of an empirical model for $\overline{(\delta u)^n}$, which complies with $\overline{(\delta u)^n} \sim r^{n/3}$ as $Re_\lambda \to \infty$, shows that the finite Reynolds number effect may differ between even- and odd-orders of $\overline{(\delta u)^n}$. This suggests that different values of Re_λ may be required between even and odd values of n for compliance with $\overline{(\delta u)^n} \sim r^{n/3}$. The model describes adequately the dependence on Re_λ of the available experimental data for $\overline{(\delta u)^n}$ and supports indirectly the extrapolation of these data to infinitely large Re_λ.

Key words: turbulence theory

† Email address for correspondence: shunlin.tang88@gmail.com

1. Introduction

For the second- and third-order velocity structure functions in the inertial range (IR), the second similarity hypothesis of Kolmogorov (1941*a*,*b*) (or K41) predicts

$$\overline{(\delta u)^2} = A_2(\bar{\varepsilon} r)^{2/3}, \tag{1.1}$$

where u is the longitudinal velocity fluctuation in the direction x, $\delta u = u(x+r) - u(x)$, r being the separation in the direction x; the overbar denotes time averaging; A_2 is a universal constant; and $\bar{\varepsilon}$ is the mean dissipation rate of the turbulent kinetic energy. Also in the same range, one has

$$\overline{(\delta u)^3} = -\tfrac{4}{5}\bar{\varepsilon} r, \tag{1.2}$$

a result known as the 4/5 law, derived rigorously by K41 from the Kármán–Howarth (or KH) equation after assuming that viscosity and the influence of the large scales can be neglected. These assumptions seem plausible when the Reynolds number is infinitely large. The extent of the IR is described by $\eta \ll r \ll L$, where $\eta = (\nu^3/\bar{\varepsilon})^{1/4}$ is the Kolmogorov length scale and L is the integral length scale, defined by $L = u'^{-2}\int_0^\infty \overline{u(x+r)u(x)}\,\mathrm{d}r$, where $\overline{u(x+r)u(x)}$ is the longitudinal correlation function. Within the framework of K41, a general expression for $\overline{(\delta u)^n}$ in the IR is

$$\overline{(\delta u)^n} = A_n(\bar{\varepsilon} r)^{n/3}, \tag{1.3}$$

(hereafter denoted n-thirds law), where A_n are universal constants. Kolmogorov (1962) or K62 (see also Oboukhov 1962) made, in a response to Landau's remark (Landau & Lifshitz 1987), an important modification to (1.3), arguably to account for the effect of the large-scale motion on the IR. This has since been widely attributed to the intermittency of ϵ (Sreenivasan & Antonia 1997). Equation (1.3) was replaced by

$$\frac{\overline{(\delta u)^n}}{u'^n} \sim \left(\frac{r}{L}\right)^{\zeta_n}, \tag{1.4}$$

where $u' \equiv \overline{u^2}^{1/2}$. Like (1.1) and (1.2), both (1.3) and (1.4) are expected to be valid only when $Re_\lambda \to \infty$. Except when $n = 3$, the premultipliers in (1.4) should not depend on the Reynolds number but may be affected by the macrostructure of the flow. As in (1.3), the exponents ζ_n are universal. The value of ζ_3 remains equal to 1, in compliance with (1.2). For $n \neq 3$, the magnitude of ζ_n can now depart from $n/3$. This departure or anomalous scaling, which seems to be relatively well described by the relation $\zeta_n = n/9 + 2\left[1 - (2/3)^{n/3}\right]$ (She & Leveque 1994), has received fairly strong support from both experimental and numerical data in a wide range of turbulent flows. In their review, Sreenivasan & Antonia (1997) described the support as 'overwhelming' but underlined that there are several uncertainties associated with the estimation of ζ_n, not the least of which is the issue of 'how one defines the scaling range and obtains scaling exponents from power-laws of modest quality.' For example, an extended self-similarity approach (Benzi *et al.* 1993) was frequently used to extract the scaling exponents of $\overline{(\delta u)^n}$ in the literature and the resulting exponents appear to agree with the predictions of She & Leveque (1994). However, as demonstrated by Tang *et al.* (2017), this approach masks the finite Reynolds number effect on the scaling exponents of $\overline{(\delta u)^n}$ (see the discussion in the text of figure 17 of Tang *et al.* 2017). A major consideration is whether an IR is actually realizable for all available experimental and numerical data, for which the Reynolds number is finite.

The studies of Qian (1997), Qian (1999), Lundgren (2002), Lundgren (2003), Antonia & Burattini (2006), Tchoufag, Sagaut & Cambon (2012), Antonia *et al.* (2019) and Meldi, Djenidi & Antonia (2021) have indicated that (1.2) is in fact approached very slowly, so that a very large value of Re_λ ($= u'\lambda/\nu$, where $\lambda = u'/(\partial u/\partial x)'$ and ν is the fluid kinematic viscosity) may be required before the IR is unambiguously established (see figure 4.6 of Sagaut & Cambon (2018) which summarizes different predictions for $\overline{(\delta u)^3}$). In particular, the eddy damped quasinormal Markovian numerical simulations in both decaying and forced homogeneous isotropic turbulence (Meldi *et al.* 2021) support Antonia & Burattini (2006) and Antonia *et al.* (2019). This seriously calls into question the validity of the published estimates of ζ_n. There is compelling evidence (Tang *et al.* 2017) to suggest that the finite Reynolds number (FRN) effect needs to be taken into account, since $\overline{(\delta u)^n}$, regardless of how it is normalized, continues to evolve with Re_λ in the scaling range.

One expects that, as described by Kolmogorov's first similarity hypothesis, the behaviour of the small scales is characterized by $\bar{\varepsilon}$ and ν. The relevant scales are η and u_K ($= (\nu\bar{\varepsilon})^{1/4}$). In the energy containing range of separations, the relevant scales are expected to be u' and L. This dual scaling is expected to apply, albeit in an approximate fashion, at finite values of Re_λ. As Re_λ continues to increase, there should be a region of overlap between the two different normalizations. When $Re_\lambda \to \infty$, the IR should be established rigorously and the two sets of scales should become interchangeable in this range.

Gamard & George (2000) used this dual scaling approach to describe how the longitudinal velocity spectrum, as measured by Mydlarski & Warhaft (1996) in decaying turbulence downstream of an active grid, evolves with Re_λ in the overlap region. In this region, the spectrum was assumed to vary, albeit approximately, as $\alpha k_1^{-5/3+\beta}$, where α and β depend on Re_λ. In the limit $Re_\lambda \to \infty$, $\beta \to 0$ and $\alpha \to$ constant, a result (Obukhov 1941) which corresponds to (1.1). The latter equation was derived, starting with the Kármán–Howarth equation, by Lundgren (2002) using matched asymptotic expansions. In essence, this approach is not dissimilar to using dual scaling, since outer and inner expansions satisfy similarity based on (u', L) and (u_K, η), respectively. Lundgren (2002) noted that this derivation of the 2/3 law is similar to Millikan's derivation of the log law in turbulent wall flows (Millikan 1939). This analogy was also noted by Barenblatt & Goldenfeld (1995), Barenblatt & Chorin (1998) and McKeon & Morrison (2007). Djenidi, Antonia & Tang (2019) showed that scale invariance leads to the 'n-thirds' law when $Re_\lambda \to \infty$. More recently, Djenidi, Antonia & Tang (2022) and Djenidi, Antonia & Tang (2023) found that constraints imposed by the Cauchy–Schwarz inequality require ζ_n to be equal to $n/3$ when $Re_\lambda \to \infty$. Equation (1.3) conforms with this requirement but (1.4) violates it if $\zeta_n \neq n/3$.

Grid turbulence, which represents a close, though imperfect, approximation to homogeneous isotropic turbulence is expected to satisfy dual scaling. This has already been verified by Mydlarski & Warhaft (1996) and Gamard & George (2000) in the context of the u spectrum, which corresponds to $\overline{(\delta u)^2}$, for values of Re_λ extending to approximately 470. These authors found, by extrapolation of Re_λ to infinity, that the data comply with (1.1). The appropriateness of this result is all the more compelling, in the context of the dual scaling, when it is recognized that the KH equation satisfies similarity at all scales as $Re_\lambda \to \infty$ (e.g. Speziale & Bernard 1992). It is clearly important to test the dual scaling approach to larger values of both Re_λ and n. This is the main objective of this paper. For this purpose, we make use of the published data for $\overline{(\delta u)^n}$ obtained in the variable density turbulent tunnel (VDTT) facility at the Max Planck Institute in Göttingen (Bodenschatz *et al.* 2014). The distributions of $\overline{(\delta u)^n}$ as a function of r have appeared in

several publications (e.g. Bodenschatz *et al.* 2014; Sinhuber, Bodenschatz & Bewley 2015; Sinhuber, Bewley & Bodenschatz 2017; Birnir 2019; Kaminsky *et al.* 2020) for $2 \leq n \leq 8$ and values of Re_λ as large as approximately 1500.

In § 2, we first examine the appropriateness of the dual scaling approach in the context of the Kármán–Howarth equation (i.e. the transport equation of $\overline{(\delta u)^2}$) for two cases: first, when the contribution of the large-scale term is neglected, and second, when the contribution from the viscous term is neglected. In § 3, we briefly recall the basic parameters for the VDTT grid turbulence data. In § 4, we test the VDTT data in the context of the dual scaling. We next present a model for $\overline{(\delta u)^n}$ which complies with the dual scaling. In particular, the model is constrained to yield a power-law behaviour ($\sim r^{\zeta_n}$, with $\zeta_n = n/3$) when $Re_\lambda \to \infty$. The adequate agreement between the model and the data (§ 5) allows extrapolation via the model to values of Re_λ that are several orders of magnitude larger than in the experiment. Conclusions are given in § 6.

2. Dual scaling in the context of the Kármán–Howarth equation

We consider first the applicability of the inner (Kolmogorov scales, η and u_K) and outer (u' and L) scaling in the context of the Kármán–Howarth equation which governs the transport of $\overline{(\delta u)^2}$:

$$\frac{4}{5}\bar{\epsilon} r = -\overline{(\delta u)^3} + 6\nu \frac{\partial}{\partial r}\overline{(\delta u)^2} + I_u(r), \tag{2.1}$$

where $I_u(r)$ is the term which reflects the contribution from the large scales to the transport of $\overline{(\delta u)^2}$ in homogeneous and isotropic turbulence (e.g. Danaila *et al.* 1999; Hill 2001). We will focus on decaying grid turbulence, partly because this flow can satisfy isotropy, at least for small scales, to a reasonable approximation and also because moderately large values of Re_λ can be achieved, e.g. by using an active grid (e.g. Mydlarski & Warhaft 1996, 1998; Gylfason, Ayyalasomayajula & Warhaft 2004) or by varying the density of the fluid (e.g. Bodenschatz *et al.* 2014; Sinhuber *et al.* 2015, 2017; Kaminsky *et al.* 2020). The departure from local isotropy at all scales can be quantified by the ratio between calculated and measured second-order spanwise velocity structure functions, i.e. $\overline{(\delta w)^2}_{iso}/\overline{(\delta w)^2}$, where $\overline{(\delta w)^2}_{iso}$ is given by (Monin & Yaglom 2007)

$$\overline{(\delta w)^2}_{iso} = \left(1 + \frac{r}{2}\frac{\mathrm{d}}{\mathrm{d}r}\right)\overline{(\delta u)^2}. \tag{2.2}$$

At $r = \lambda$, a separation which resides near the lower end of the scaling range (Tang *et al.* 2017), the departure from local isotropy is relatively small ($\lesssim 10\,\%$, see figure 10 of Lavoie, Djenidi & Antonia (2007) at $Re_\lambda = 36$–43 in grid turbulence with and without a secondary contraction). Further, it was shown that the ratio $\overline{(\delta w)^2}_{iso}/\overline{(\delta w)^2}$ satisfies isotropy within approximately $10\,\%$ at all separations when a secondary contraction is introduced. This result is consistent with that of Comte-Bellot & Corrsin (1966) and Comte-Bellot & Corrsin (1971) who used a contraction to improve the isotropy of grid turbulence, with u' being nearly equal to v'. It is worth mentioning that since the magnitude of Re_λ in the present paper is much larger than that of Lavoie *et al.* (2007), we thus expect a further improved local isotropy, compared with that of Lavoie *et al.* (2007). Also, since isotropy requires homogeneity, and isotropy at all scales is approximately satisfied in grid turbulence, the weak spatial decay along x, the mean flow direction, should not affect the behaviour of $\overline{(\delta u)^n}$. In other words, the influence of any small inhomogeneity in the x

direction on the behaviour of $\overline{(\delta u)^n}$ should be negligible. Further, it is well established, based on the KH equation, that the effect of the spatial decay along the x direction in the scaling range weakens as Re_λ increases (Antonia & Burattini 2006; Tang *et al.* 2017; Antonia *et al.* 2019). A further attractive feature of grid turbulence is that the energy budget is relatively simple and can hence be measured fairly accurately thus yielding a reliable estimation of $\bar{\varepsilon}$ (e.g. Antonia, Zhou & Zhu 1998).

The two main items of interest here are the conditions for which inner (or Kolmogorov) scaling (u_K, η) and outer scaling (u', L) satisfy the similarity of (2.1).

(i) When the effect of the large scale term $I_u(r)$ is neglected, the similarity of (2.1) is readily satisfied by

$$\frac{\overline{(\delta u)^2}}{u_0^2} = f\left(\frac{r}{l_0}\right), \tag{2.3}$$

$$\frac{\overline{(\delta u)^3}}{u_0^3} = g\left(\frac{r}{l_0}\right), \tag{2.4}$$

when $u_0 \equiv u_K$ and $l_0 \equiv \eta$, *viz.* the (u_K, η) scaling applies. This was discussed in some detail by Antonia, Djenidi & Danaila (2014). Equation (2.1) can be rewritten as

$$\frac{4}{5}\frac{r}{l_0} = \frac{6\nu u_0^2}{\bar{\epsilon} l_0^2} f' - \frac{u_0^3}{\bar{\epsilon} l_0} g\left(\frac{r}{l_0}\right) \tag{2.5}$$

(here, the prime signifies a derivative with respect to r/l_0), so that $\bar{\varepsilon} l_0/u_0^3$ and $\bar{\varepsilon} l_0^2/\nu u_0^2$ (or $\bar{\varepsilon} l_0/u_0^3$, $u_0 l_0/\nu$) are constants. Clearly, (u_K, η) is a possible solution since

$$\frac{\bar{\varepsilon}\eta}{u_K^3} = 1 \quad \text{and} \quad \frac{u_K \eta}{\nu} = 1. \tag{2.6a,b}$$

Scaling based on (u', L) is also possible provided

$$\frac{\bar{\epsilon} L}{u'^3} = C_\epsilon = \text{constant} \quad \text{and} \quad \frac{u' L}{\nu} = \text{constant}. \tag{2.7a,b}$$

The first requirement in (2.7*a*,*b*) has been validated in several different flows (e.g. Sreenivasan 1984; Burattini, Lavoie & Antonia 2005*b*; Ishihara, Gotoh & Kaneda 2009; Mi, Xu & Zhou 2013; Vassilicos 2015; McComb *et al.* 2015), at least when Re_λ is sufficiently large. The second can, to our knowledge, hold only in the far field of a circular jet (Antonia, Satyaprakash & Hussain 1980; Burattini, Antonia & Danaila 2005*a*) when Re_λ is finite. It should however be satisfied in decaying grid turbulence when $Re_\lambda \to \infty$ (e.g. George 1992; Speziale & Bernard 1992; Antonia *et al.* 2003). The above observations lead to the conclusion that the scaling (u_K, η) should be effective regardless of the flow since the two dimensionless parameters in (2.6*a*,*b*) are indeed universal (with a value of 1). Nevertheless, the neglect of the large-scale term (2.5) for values of r/η that extend into the IR is unlikely to be fully justifiable unless $Re_\lambda \to \infty$. Neither of the parameters in (2.7*a*,*b*) is likely to be flow independent; indeed, there is adequate evidence (e.g. Sreenivasan 1984; Burattini *et al.* 2005*b*; Mi *et al.* 2013; Vassilicos 2015) that the magnitude of C_ϵ depends on the flow.

(ii) $I_u(r)$ is now retained and the viscous term in (2.1) is neglected. The focus now is on the larger scales of motion. Equation (2.1) can be rewritten as

$$\frac{4}{5}\frac{r}{l_0} = -\frac{u_0^3}{\bar{\varepsilon} l_0} g\left(\frac{r}{l_0}\right) + \frac{I_u(r)}{\bar{\varepsilon} l_0}. \tag{2.8}$$

We concentrate on grid turbulence, for which

$$I_u(r) = -\frac{3}{r^4}\int_0^r s^4 \left[U\frac{\partial \overline{(\delta u)^2}}{\partial x}\right] \mathrm{d}s, \tag{2.9}$$

where s is a dummy variable, identifiable with the separation along x, and U is the (constant) mean velocity in the x direction (e.g. Danaila *et al.* 1999; Antonia *et al.* 2000; Danaila, Anselmet & Antonia 2002). Using (2.9), $I_u/\bar{\varepsilon} l_0$ becomes

$$\frac{3}{(r/l_0)^4}\left(\int_0^{r/l_0}\left(\frac{s}{l_0}\right)^4 f\left(\frac{r}{l_0}\right)\frac{\mathrm{d}s}{l_0}\right)\left[\frac{U}{\bar{\varepsilon}}\frac{\partial u_0^2}{\partial x} - \frac{U u_0^2}{\bar{\varepsilon}}\left(\frac{r}{l_0}\right)^2 \frac{f'}{l_0}\frac{\mathrm{d}l_0}{\mathrm{d}x}\right]. \tag{2.10}$$

The expression within square brackets must be constant for similarity to be satisfied. The first term of this expression is indeed constant since $\bar{\epsilon} = -\frac{3}{2}U(\partial u_0^2/\partial x)$ is the turbulent energy budget (when $u_0 \equiv u'$). The second term is also constant with the (u', L) scaling since $\bar{\varepsilon}L/u'^3$ is constant and $(1/u')(\mathrm{d}L/\mathrm{d}x)$ is also constant as both u' and $\mathrm{d}L/\mathrm{d}x$ vary as $x^{n/2}$ when the energy decays according to a power-law, *viz.* $\overline{u^2} \sim x^n$ and $\bar{\epsilon} \sim x^{n-1}$; the latter two relations, together with $C_\varepsilon = \bar{\epsilon}L/u'^3 = \text{const}$, lead to $L \sim x^{n/2+1}$. It is worth mentioning that U in the second term within the square brackets does not affect the above analysis and the corresponding results since we can replace $U/\mathrm{d}x$ with $1/\mathrm{d}t$ in grid turbulence. The previous similarity requirements were previously outlined by Kármán & Von Howarth (1938) and Townsend (1976). We conclude that the similarity of (2.8), i.e. the transport equation of $\overline{(\delta u)^2}$ when r is sufficiently large to allow the viscous term to be neglected, is satisfied by the (u', L) scaling. We should note however that the (u_K, η) scaling can also satisfy similarity of (2.8) when $n = -1$ (in this case, both $(1/\bar{\varepsilon})(\partial u_K^2/\partial x)$ and $(1/u_K)(\partial \eta/\partial x)$ are constant). This rate of decay was shown by Speziale & Bernard (1992) to be the asymptotically consistent high-Reynolds-number solution. The condition $u'L/\nu = \text{constant}$ in (2.7*a*,*b*) is immediately satisfied in this case so that the scales (u', L), just like (u_K, η), would satisfy complete similarity (or self-preservation), i.e. similarity for all scales of motion. The Taylor microscale λ should then be a valid replacement for L since Re_λ should no longer depend on x and λ should be proportional to L. The general self-preservation analysis of Djenidi & Antonia (2015) confirmed the dependence of n on the initial conditions and showed how this dependence is related to the initial length and velocity scales. These authors suggested that it may be possible to have initial conditions that lead to $n = -1$ with a finite Re_λ. However, Re_λ must remain constant throughout the decay.

The available grid turbulence data in the literature indicate that n is typically smaller than -1, usually with a value ranging between -1.1 and -1.5 (e.g. George 1992; Lavoie *et al.* 2007; Lee *et al.* 2013; Sinhuber *et al.* 2015). In particular, Sinhuber *et al.* (2015) showed that n is independent of the Reynolds number, with a value of $n = -1.18 \pm 0.02$, over a wide range of Reynolds numbers; this value is close to the prediction of Saffman (1967) ($n = -1.2$). Lavoie *et al.* (2007) showed experimentally that even when the turbulence is nearly perfectly isotropic, n is not equal to -1. Our interest is to assess the validity of the dual scaling and the range of r/l_0 over which it applies. The scaling based

on $(u_K,\ \eta)$ is expected to extend to increasingly larger values of r/η as Re_λ increases. Correspondingly, the scaling based on $(u',\ L)$ is expected to extend to increasingly smaller values of r/L as Re_λ increases. Since both scalings must eventually overlap as $Re_\lambda \to \infty$, the overlap region should include the inertial range. Regardless of the scaling used, this overlap region should satisfy similarity and hence be independent of Re_λ. All of the above analysis is focused on the grid turbulence where the influence of large scales on $-\overline{(\delta u)^3}$ can be quantified by the $I_u(r)$ term in (2.9). If one considers different flows with different large-scale forcing, the influence of the large-scale motion is likely to differ from that in grid turbulence. Accordingly, in those situations, the flow may locally reflect the large-scale anisotropy at finite Re_λ imposed by the forcing. For example, when anisotropic forcing is used in direct numerical simulations of box turbulence at $Re_{q\lambda} = 20$–32 $(= \overline{u_i u_i}^{1/2}\lambda/\nu)$, it induces small-scale anisotropy which is traced to the dynamics of non-local triads with one low wavenumber in the directly forced wavenumber band (Yeung & Brasseur 1991). Also, Kurien & Sreenivasan (2000) observed that the structure functions of order two to six exhibit a strong anisotropy at moderate scales in the atmospheric surface layer at $Re_\lambda = 870$–2100.

3. Basic flow parameters in grid turbulence

The grid turbulence data we used for our study were digitized from figures presented by Bodenschatz *et al.* (2014) and Kaminsky *et al.* (2020) ($Re_\lambda = 110$–1620). Since all the experimental data reported here have already been published, the reader can find detailed descriptions of the experimental conditions and measurement techniques in the original papers. Here we only describe and discuss the basic flow parameters associated with those two datasets and explain the treatment we have had to apply to these data.

Bodenschatz *et al.* (2014) estimated $\bar{\varepsilon}$ from $\overline{(\delta u)^3}$ by assuming $\bar{\varepsilon} = \max(-5/4\overline{(\delta u)^3}/r)$, i.e. assuming that (1.2) is tenable. This would result in $\bar{\varepsilon}$ being underestimated since the maximum value of $\overline{(\delta u)^3}/\bar{\varepsilon} r$ has not yet reached the value of 4/5 for the available data in grid turbulence (see for example figure 1*a* of Antonia *et al.* (2019)). Indeed, their magnitudes of C_ϵ $(\equiv \bar{\varepsilon} L/u'^3 = 0.58,\ 0.71,\ 0.83,\ 0.77,\ 0.77$ and 0.75 at $Re_\lambda = 150,\ 400,\ 549,\ 730,\ 1370$ and 1620, respectively, Bodenschatz *et al.* 2014) are smaller than those of Kaminsky *et al.* (2020) ($C_\varepsilon = 1.06,\ 1.12,\ 0.91,\ 0.91$ and 0.81 at $Re_\lambda = 110,\ 264,\ 508,\ 1000$ and 1450, respectively), in which $\bar{\varepsilon}$ was estimated from the turbulent energy budget $\bar{\epsilon} = -\frac{3}{2}U(\partial u'^2/\partial x)$. Also, the spectra of Bodenschatz *et al.* (2014) in the dissipative range do not collapse, see figure 1(*b*), which is reproduced from their figure 30. To obtain a more accurate estimation of $\bar{\epsilon}$, the spectral chart method of Djenidi & Antonia (2012) has been applied to the spectra of Bodenschatz *et al.* (2014) (their figure 30, or figure 1(*b*) in the present paper). The 'new' estimates of $\bar{\varepsilon}$ are denoted by $\bar{\varepsilon}_{spec}$. This method is based on the observation that there is collapse in the upper part of the dissipative range not only for grid turbulence, but also for many other turbulent flows; see for example figure 9 of Saddoughi & Veeravalli (1994), figure 6.14 of Pope (2000), figure 3 of Gotoh, Fukayama & Nakano (2002), figure 5 of Larssen & Devenport (2011), figures 1–2 of Antonia *et al.* (2014) and figure 1(*a*) of Tang *et al.* (2020). Therefore, the values of $\bar{\varepsilon}_{spec}$ ensure that there is collapse in the upper part of the dissipative range, as illustrated in figure 1(*a*) where the distributions are normalized by $\bar{\varepsilon}_{spec}$ and ν. For comparison, we have included the grid turbulence data of Larssen & Devenport (2011) at $Re_\lambda = 124$ and 1360. It is worth mentioning that all the data of Bodenschatz *et al.* (2014) were obtained in passive grid turbulence. However, the data of Larssen & Devenport (2011) at $Re_\lambda = 124$ and 1362 were measured in passive and active grid turbulence, respectively.

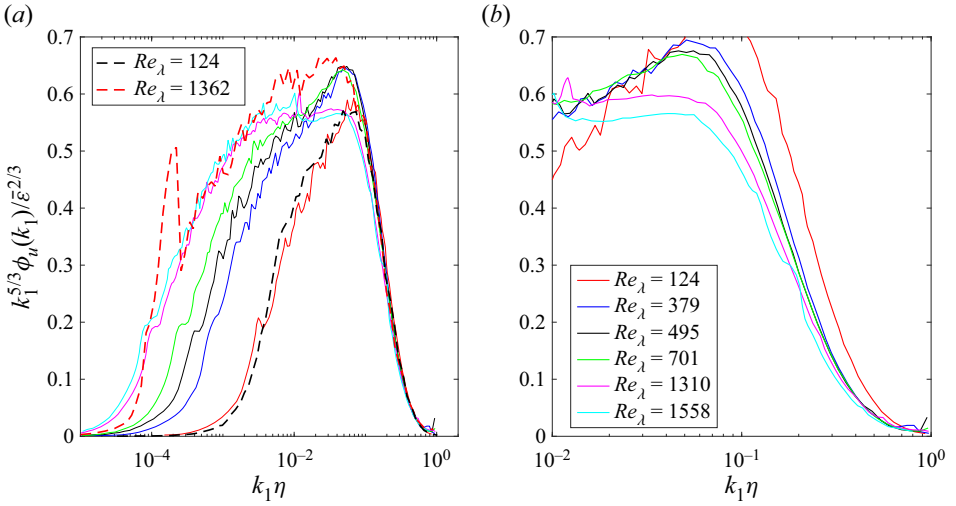

Figure 1. (*a*) Kolmogorov normalized compensated spectra of u in grid turbulence (Bodenschatz *et al.* 2014) ($Re_\lambda = 110$–1450), normalized by $\bar{\epsilon}_{spec}$ and ν (the spectral chart method). For comparison, we have included the grid turbulence data of Larssen & Devenport (2011) (dashed curves) at $Re_\lambda = 124$ and 1360. (*b*) Corresponding grid turbulence data of Bodenschatz *et al.* (2014) ($Re_\lambda = 110$–1450), normalized by $\bar{\epsilon}$, estimated from $\overline{(\delta u)^3}$ (see text), and ν; note that to see the dissipative range more clearly, a smaller range $k_1\eta = 0.01$–1 is used for the vertical axis.

The distribution of Bodenschatz *et al.* (2014) is in almost perfect agreement with that of Larssen & Devenport (2011) at $Re_\lambda = 124$ at all scales. This is not too surprising since both distributions were measured in passive grid turbulence at the same Re_λ. We can observe that there is a large spike at low wavenumbers (around $k_1\eta \approx 0.0002$) for the data of Larssen & Devenport (2011) at $Re_\lambda = 1362$. This is due to the rotation of the active grid which 'introduces additional energy into the spectra' (Larssen & Devenport 2011). It is plausible that this spike, which reflects the presence of a strong coherent motion, may affect the medium wavenumber range, i.e. $0.002 \lesssim k_1\eta \lesssim 0.04$, over which the magnitude of the energy spectrum at $Re_\lambda = 1362$ is larger than all others. We recall that Larssen & Devenport (2011) calculated $\bar{\varepsilon}$ by integrating the longitudinal dissipation spectrum, i.e. $\bar{\varepsilon} = 15\nu \int k_1^2 \phi_u(k_1) dk_1$. Local isotropy requires that the integration of the Kolmogorov-normalized longitudinal dissipation spectrum is equal to 1/15 ($\equiv 0.0667$). Although not shown here, we should stress that the dissipation spectrum at $Re_\lambda = 1362$ is in good agreement with all other distributions at all scales for $Re_\lambda \leq 701$, confirming the accuracy of the dissipation spectrum at $Re_\lambda = 1362$. More importantly, the integration across all scales at $Re_\lambda = 1362$ leads to 0.069, which is only 3.5 % larger than the isotropic value of 1/15. This further indicates that the magnitude of $\bar{\varepsilon}$ at $Re_\lambda = 1362$ should be reasonably accurate. More importantly, there is reasonable agreement between the '$\bar{\varepsilon}_{spec}$'-normalized spectra and the spectra of Larssen & Devenport (2011) for $k_1\eta \gtrsim 0.3$ at all Re_λ. In contrast, as seen in figure 1(*b*), there is no collapse in the upper part of the dissipative range since $\bar{\epsilon}$ was underestimated by using the maximum value of $-\overline{(\delta u)^3}/\bar{\varepsilon} r$ at finite Re_λ. In particular, as Re_λ increases, the approach to a $-5/3$ scaling of the spectra, as reflected by the nearly horizontal distributions, is similar to that of Mydlarski & Warhaft (1996). The magnitudes of C_ε, based on $\bar{\varepsilon}_{spec}$, are close to those of Kaminsky *et al.* (2020) (figure 2), confirming that $\bar{\varepsilon}_{spec}$ should be very close to the true value $\bar{\varepsilon}$. To further confirm the magnitudes of $\bar{\varepsilon}_{spec}$, we have also included the grid turbulence data of Comte-Bellot &

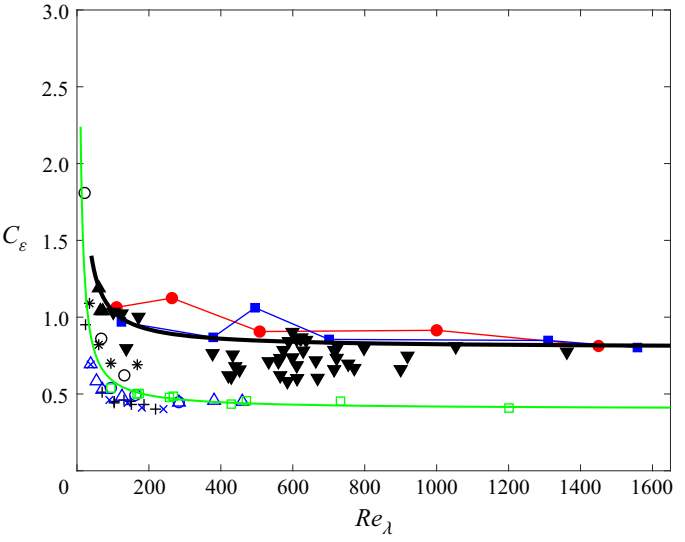

Figure 2. Distributions of $C_\epsilon = \bar{\epsilon}L/u'^3$ versus Re_λ in grid turbulence. (● red), (Kaminsky *et al.* 2020); (■ blue), re-estimated C_ϵ, based on $\bar{\varepsilon}_{spec}$ (the spectral chart method), versus Re_λ for the data of Bodenschatz *et al.* (2014) (see text). For comparison, we have included the grid turbulence data of Comte-Bellot & Corrsin (1971) (▲) and Larssen & Devenport (2011) (▼). Black curve, (3.1) with $A = 0.4$ and $B = 60$. Also included are the data in stationary forced periodic box turbulence ((◯ black), Wang *et al.* (1996); (◯ blue), Ishihara & Kaneda (2002); (∗ black), Jimenez *et al.* (1993); (□ green), Ishihara *et al.* (2009); (+ black), Cao, Chen & Doolen (1999); (× blue), Yeung & Zhou (1997); (△ blue), Gotoh *et al.* 2002). Green curve, (3.1) with $A = 0.2$ and $B = 92$.

Corrsin (1971) ($Re_\lambda = 61$–72, ▲) and Larssen & Devenport (2011) ($Re_\lambda = 101$–1362, ▼)) (see figure 2). We can observe that the magnitudes of C_ε, based on $\bar{\varepsilon}_{spec}$, are also close to those of Comte-Bellot & Corrsin (1971) and Larssen & Devenport (2011), especially for $Re_\lambda \lesssim 300$ and $Re_\lambda \gtrsim 900$; the scatter for the data of Larssen & Devenport (2011) in the range $300 \lesssim Re_\lambda \lesssim 900$ is relatively large. We recall that C_ε in stationary forced periodic box turbulence follows a functional form (Donzis, Sreenivasan & Yeung 2005):

$$C_\varepsilon = A(1 + \sqrt{1 + (B/Re_\lambda)^2}), \tag{3.1}$$

where $A = 0.2$ and $B = 92$ (see green curve in figure 2). When using (3.1) to fit the grid turbulence data in figure 2, we observe that the asymptotic value of C_ε in grid turbulence is approximately 0.8, which corresponds to $A = 0.4$. Here, B is essentially constant which reflects the finite Reynolds number effect on C_ε in this flow. We take $B = 60$ which appears to fit all the grid turbulence data reasonably well. We finally compare the $\overline{(\delta u)^2}/u_K^2$ distributions, calculated from the Kolmogorov-normalized energy spectra (figure 1*a*) using the following relation (e.g. Dickey & Mellor 1979; Monin & Yaglom 2007):

$$\overline{(\delta u)^2}/u_K^2 = 2\int_0^\infty \phi_u(k_1\eta)(1 - \cos(k_1 r))\,\mathrm{d}(k_1\eta), \tag{3.2}$$

with the other grid turbulence data (Comte-Bellot & Corrsin 1971; Malecot 1998; Zhou & Antonia 2000; Larssen & Devenport 2011) (see figure 3). Evidently, the distributions of Kaminsky *et al.* (2020) are quite close to the other grid turbulence data at all scales when Re_λ is comparable and in the dissipative range, regardless of Re_λ. Based on the above analysis, we can conclude that the magnitudes of $\bar{\varepsilon}_{spec}$, obtained from the spectral chart

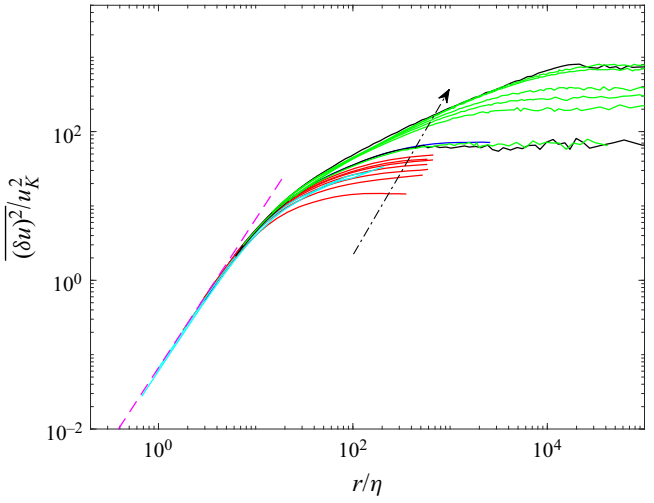

Figure 3. Distributions of $\overline{(\delta u)^2}/u_K^2$ versus r/η in grid turbulence for the data of Bodenschatz *et al.* (2014) at $Re_\lambda = 124$, 379, 495, 701, 1310 and 1558 (green curves). For comparison, other grid turbulence data are also shown; red curves, Zhou & Antonia (2000) ($Re_\lambda = 27$, 51, 62, 75, 83, 89 and 100); cyan curves, Comte-Bellot & Corrsin (1971) ($Re_\lambda = 61$ and 65); black curves, Larssen & Devenport (2011) ($Re_\lambda = 124$ and 1360); blue curve, Malecot (1998) ($Re_\lambda = 144$); pink curve, $(r/\eta)^2/15$. The arrow indicates the direction of increasing Re_λ. Note that the data of Comte-Bellot & Corrsin (1971), Larssen & Devenport (2011) and Bodenschatz *et al.* (2014) are calculated from their spectra, based on (3.2).

method, are reasonably accurate and reliable. The values of Re_λ are then re-estimated from the isotropic relation $\overline{u^2}/u_K^2 = Re_\lambda/15^{1/2}$. The final values are 124, 379, 495, 701, 1310 and 1558, which are slightly smaller than the values of Bodenschatz *et al.* (2014), i.e. $Re_\lambda =$ 150, 400, 549, 730, 1370 and 1620, respectively. For reference, we have also included the data for stationary forced periodic box turbulence. We can observe from figure 2 that C_ε is close to 0.8 at large Re_λ for the grid turbulence and to 0.4 for the stationary forced periodic box turbulence. This difference is consistent with the difference observed in L/η since C_ε can be written as

$$C_\varepsilon = \frac{\bar{\varepsilon} L}{u'^3} = \frac{L/\eta}{u'^3/u_K^3} = \frac{L/\eta}{Re_\lambda^{3/2}/15^{3/4}}, \tag{3.3}$$

where the isotropic relation $u'^2/u_K^2 = Re_\lambda/15^{1/2}$ has been used. A plausible reason for the difference in the magnitude of C_ε between grid and box turbulence is the difference in L/η at any given Re_λ, which reflects, at least partially, the different types of large-scale forcing between these two flows. For example, $L/\eta = 2522$ at $Re_\lambda = 1300$ in box turbulence (Iyer, Sreenivasan & Yeung 2020), whereas $L/\eta = 5516$ at $Re_\lambda = 1360$ in grid turbulence (Larssen & Devenport 2011). Tsuji (2009) observed a difference of a factor of two in L/η between the DNS data and experimental data in most other flows (see their figure 1*b*). This difference in L/η is equivalent to the factor of two difference in C_ε between grid turbulence and box turbulence.

Kaminsky *et al.* (2020) have shown distributions of $\overline{(\delta u)^2}$, $\overline{|\delta u|^3}$, $\overline{(\delta u)^4}$, $\overline{(\delta u)^6}$ and $\overline{(\delta u)^8}$ in grid turbulence at $Re_\lambda = 110$, 264, 508, 1000 and 1450, respectively; the $\overline{(\delta u)^2}/u_K^2$ distributions are shown in figure 4(*a*) (green curves). Figures 1–5 of Kaminsky *et al.* (2020) were digitized to obtain $\overline{(\delta u)^2}$ distributions. We then divided $\overline{(\delta u)^2}$ by u_K^2 (u_K was calculated from η and ν shown in their table 1). For comparison, also included are the

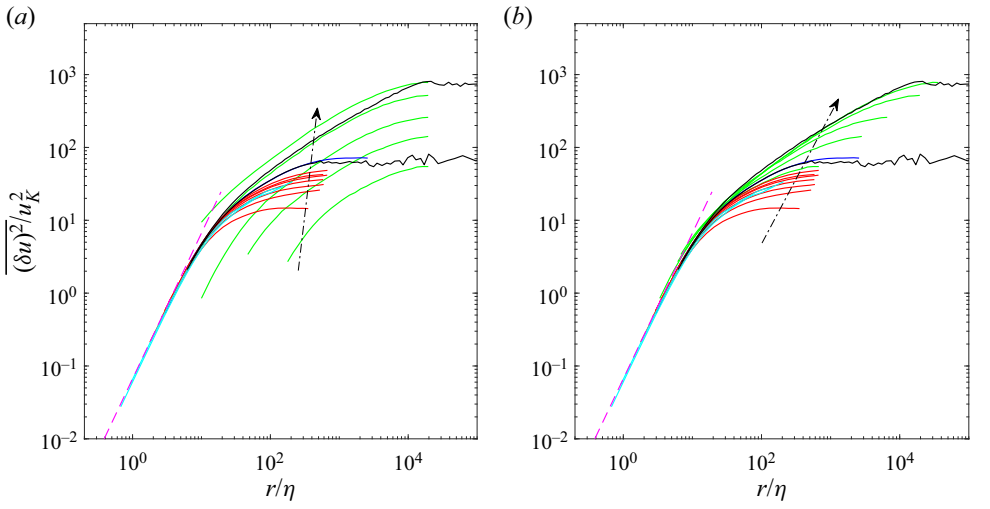

Figure 4. (*a*) Distributions of $\overline{(\delta u)^2}/u_K^2$ versus r/η in grid turbulence for the data of Kaminsky *et al.* (2020) at $Re_\lambda = 110$, 264, 508, 1000 and 1450 (green curves). Panel (*b*) corresponds to the same data, after applying a numerical factor M to their data (see text). For comparison, other grid turbulence data, same as in figure 3, are also shown in (*a*,*b*). Pink curve, $(r/\eta)^2/15$. The arrow indicates the direction of increasing Re_λ.

Re_λ	110	264	508	1000	1450
M	29	6.9	2.96	1	0.54

Table 1. Values of M used to plot $\overline{(\delta u)^2}/u_K^2$, $\overline{(\delta u)^4}/u_K^4$ and $\overline{(\delta u)^6}/u_K^6$ versus r/η at each Re_λ for the data of Kaminsky *et al.* (2020) (see text). Note that a value of 10, instead of 6.9, is used to plot $\overline{(\delta u)^4}/u_K^4$ at $Re_\lambda = 264$ since its distribution should lie between the distributions of $Re_\lambda = 110$ and 508 in the dissipative range (see figure 5).

other grid turbulence data, same as in figure 3. It can be observed that the distributions of Kaminsky *et al.* (2020) strongly depart from the other distributions. This is because they actually plotted $\overline{(\delta u)^n}/u_K^n$ versus $r/(\eta M)$, instead of $\overline{(\delta u)^n}/u_K^n$ versus r/η. We recall that there is an overwhelming amount of data confirming that the $\overline{(\delta u)^2}/u_K^2$ distributions collapse in the dissipative range over a large range of Re_λ in various flows (e.g. Pearson & Antonia 2001; Gotoh *et al.* 2002; Ishihara *et al.* 2009; McComb *et al.* 2014). The same is observed in grid turbulence (figure 3). It is then expected that the distributions of Kaminsky *et al.* (2020) should collapse with those reported in the literature, at least in the small-scale range, if one removes the factor M from the ratio $r/(\eta M)$. Since the value of M was not provided by Kaminsky *et al.* (2020), we replotted their data with $r/(\eta M)$ multiplied by different values of M so the distributions align with with other grid turbulence data (figure 4*b*). The values of M are 29, 6.9, 2.96, 1 and 0.54 at $Re_\lambda = 110$, 264, 508, 1000 and 1450, respectively; see also table 1. These values will be used to plot $\overline{(\delta u)^4}/u_K^4$ and $\overline{(\delta u)^6}/u_K^6$ versus r/η, which will be presented and discussed later. In other words, we do not use 'M' to correct η (or equivalently u_K); instead, it is simply a means of forcing agreement with the other grid turbulence data in the dissipative range. As discussed above, the universality of this range is supported by an overwhelming amount of data

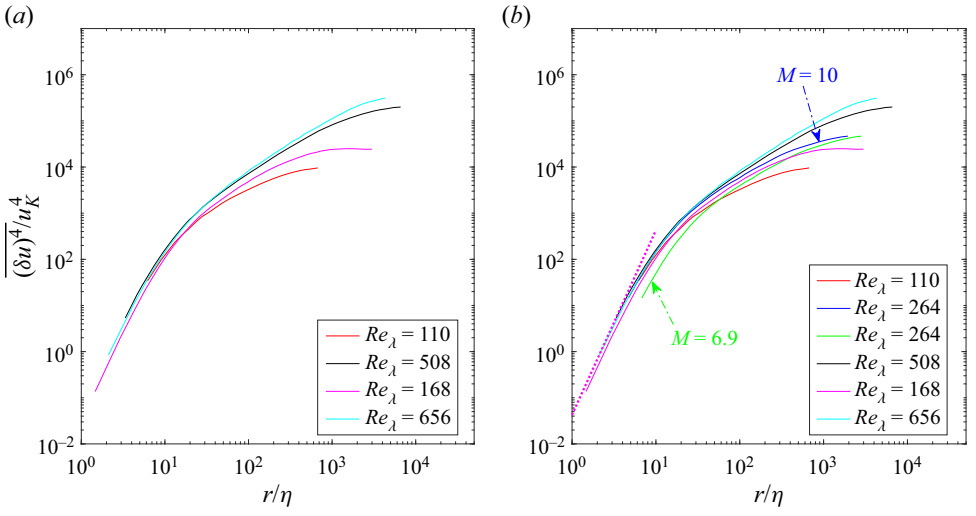

Figure 5. (*a*) Distributions of $\overline{(\delta u)^4}/u_K^4$ versus r/η in grid turbulence (Kaminsky *et al.* 2020) after applying a numerical factor $M(= 29$ and 2.96 for $Re_\lambda = 110$ and 508) to their data (see text). For comparison, the grid turbulence data of Gylfason *et al.* (2004) (without shear) at $Re_\lambda = 168$ (pink curve) and 656 (cyan curve) are shown; they are reproduced from figure 5(*c*,*d*) of Gylfason *et al.* (2004). (*b*) Distributions of $\overline{(\delta u)^4}/u_K^4$ versus r/η in grid turbulence (Kaminsky *et al.* 2020) at $Re_\lambda = 264$ after applying a numerical factor $M(= 6.9$ and 10) to their data (see text). The dotted curve, $15^{-2}F_4(r/\eta)^4$ with $F_4 = 9.6$. Other curves are the same as (*a*).

over a large range of Re_λ in various flows, as expected on the basis of the first similarity hypothesis of K41. Finally, we compare the distributions of $\overline{(\delta u)^4}/u_K^4$ at $Re_\lambda = 110$ and 508 with those of Gylfason *et al.* (2004) at comparable Re_λ (168 and 656) in grid turbulence (figure 5*a*). It is worth mentioning that $\overline{(\delta u)^4}/u_K^4$ leads to $15^{-2}F_4(r/\eta)^4$ as $r/\eta \to 1$. Also, we can observe (later from figure 16) that F_4 at $Re_\lambda = 550$ and 656 are close to each other; the same can be observed for $Re_\lambda = 110$ and 168. This implies that the distributions at $Re_\lambda = 550$ and 656 (and also those at $Re_\lambda = 110$ and 168) should be close to each other at small r/η. These two expectations are indeed observed in figure 5(*a*) in the separation range $r/\eta \lesssim 20$–30. Figure 5(*a*) further justifies our use of the numerical factor M on the data of Kaminsky *et al.* (2020). As mentioned above, $\overline{(\delta u)^4}/u_K^4$ approaches $15^{-2}F_4(r/\eta)^4$ as $r/\eta \to 1$. Also, since F_4 increases systematically with increasing Re_λ for $Re_\lambda \lesssim 500$ (see figure 16 later), the $\overline{(\delta u)^4}/u_K^4$ distribution at $Re_\lambda = 264$ at small r/η must lie between the distributions of $Re_\lambda = 110$ and 508. Yet, we can observe from figure 5(*b*) that, when $M = 6.9$, the distribution at $Re_\lambda = 264$ is smaller than that at $Re_\lambda = 110$; this is incorrect and should be rectified. The value $M = 10$, which ensures that the distribution at $Re_\lambda = 264$ at small r/η lies between the distributions of $Re_\lambda = 110$ and 508, as illustrated in figure 5(*b*), is a reasonable value for plotting $\overline{(\delta u)^4}/u_K^4$ at $Re_\lambda = 264$ (see figure 5*b*). Also, the data for $\overline{(\delta u)^8}$ are not presented in the present paper since their behaviour is similar to that of $\overline{(\delta u)^6}$. As mentioned above, Kaminsky *et al.* (2020) have also shown the $\overline{|\delta u|^3}$ distributions. In the present paper, we will only discuss the behaviour of $\overline{(\delta u)^3}$ using the data of Bodenschatz *et al.* (2014) in the same flow, instead of $\overline{|\delta u|^3}$, since there is an exact equation for the former quantity, as discussed in § 1. It is worth noting that the data mentioned above were measured by a hot-wire anemometry and Taylor's hypothesis was used to calculate $\overline{(\delta u)^n}$. It is generally accepted that this hypothesis is reliable when the

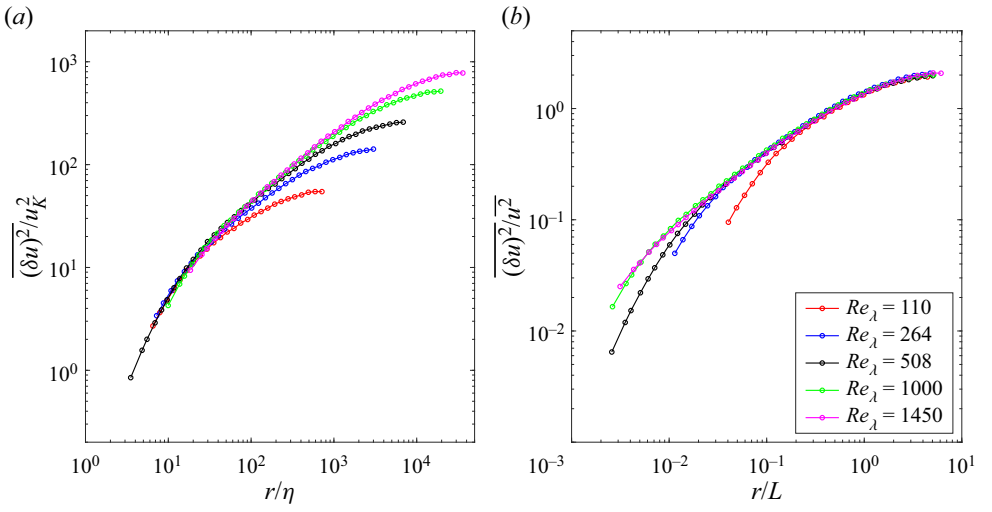

Figure 6. Effect of Re_λ on the distributions of $\overline{(\delta u)^2}$ in grid turbulence. Panels (a,b) are normalized by (u_K, η) and (u', L), respectively. These data are reproduced from Kaminsky *et al.* (2020).

mean rate of shear and turbulence intensity are small. Indeed, according to He, Jin & Yang (2017), in a flow such as grid turbulence where the mean shear rate is zero, the conversion from time to space can be written as

$$r = \sqrt{1 + (u'/U)^2}\, Ut. \tag{3.4}$$

For the VDTT grid turbulence data, the turbulence intensity u'/U is only in the range $2.35\,\% \sim 3.7\,\%$ (see table II of Bodenschatz *et al.* 2014), and thus justifies the use of Taylor's hypothesis. Pope (2000) pointed out that 'in grid turbulence with $u'/U \ll 1$, it [Taylor's hypothesis] is quite accurate.'

4. Dual scaling and its consequences

We show in figures 6–9 the distributions of $\overline{(\delta u)^n}$ ($n = 2, 3, 4, 6$) normalized by (u_K, η) and (u', L) in grid turbulence at $Re_\lambda = 110$–1558, using the data of Bodenschatz *et al.* (2014) (after reevaluating $\bar{\varepsilon}$, as discussed in § 3) and Kaminsky *et al.* (2020). We can observe from figures 6–9 that the scaling based on (u', L) extends to increasingly smaller values of r/L as Re_λ increases. Further, the scaling based on (u_K, η) extends to increasingly larger values of r/η as Re_λ increases. These results indicate that both scalings should eventually overlap at larger values of Re_λ. Another feature of figures 6–9 is that the range over which the scaling based on (u', L) is tenable appears to be larger than that over which the scaling based on (u_K, η) holds over the present Re_λ range, especially for $n > 3$. One possible reason for this behaviour is that $\overline{(\delta u)^n}/u'^n$ as $r \to L$ approaches the appropriate Gaussian values, which are Re_λ-independent, while $\overline{(\delta u)^n}/u_K^n$ as $r \to \eta$ leads to the normalized moments of the velocity derivative (F_n), which are likely to be constant only at large Re_λ for $n > 3$ (note that $F_2 = 1$ by definition and $|F_3| \approx 0.53$ for $Re_\lambda \gtrsim 300$ (Antonia *et al.* 2017)); the behaviour of F_n will be discussed briefly later in the context of figure 16. However, as $r \to \infty$, we can estimate that, for $n = 2, 4$ and 6, $\overline{(\delta u)^n}/u'^n$ approach the values of 2, 12 and 120, respectively, when (3.1), (3.7) and (3.10) of Pearson & Antonia (2001) are used. The Re_λ dependence of the limiting values of $\overline{(\delta u)^n}/u_K^n$ ($n = 2, 3, 4, 6$) as $r \to \infty$ has

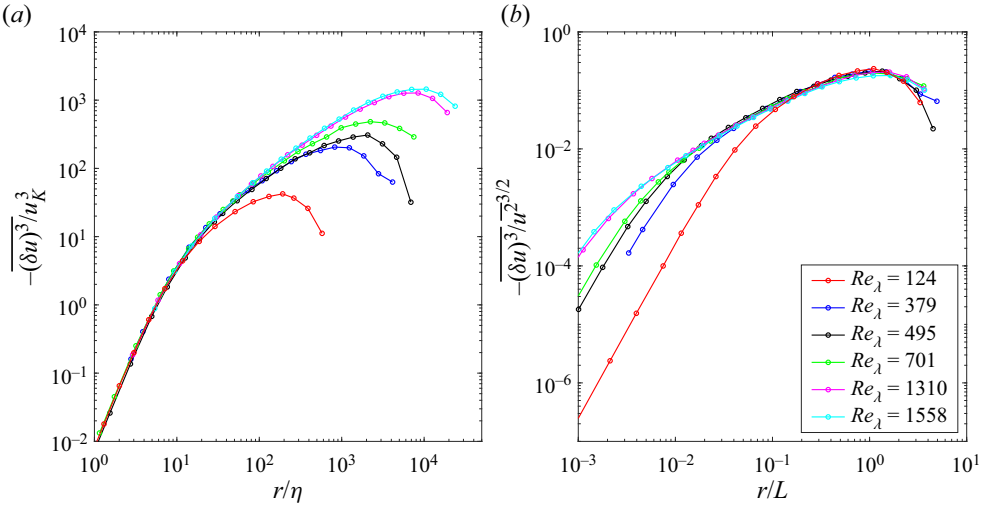

Figure 7. Effect of Re_λ on the distributions of $-\overline{(\delta u)^3}$ in grid turbulence. Panels (*a*,*b*) are normalized by (u_K, η) and (u', L), respectively. These data are reproduced from Bodenschatz *et al.* (2014); note that for (*a*), u_K and η were re-evaluated as explained in the text.

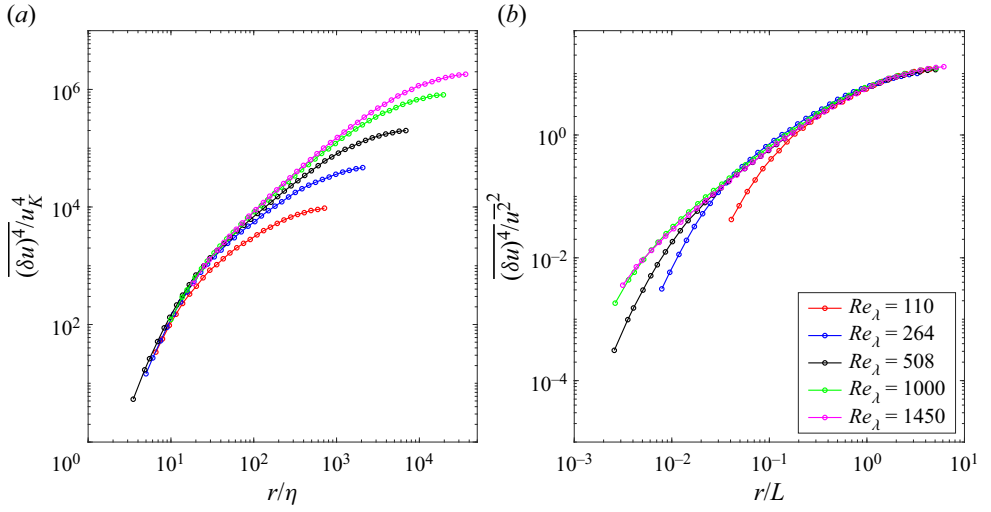

Figure 8. Effect of Re_λ on the distributions of $\overline{(\delta u)^4}$ in grid turbulence. Panels (*a*,*b*) are normalized by (u_K, η) and (u', L), respectively. These data are reproduced from Kaminsky *et al.* (2020).

been discussed by Pearson & Antonia (2001) (see their figure 6). They concluded that the assumption that δu is 'Gaussian when r is large is, experimentally, almost impossible to disprove'.

The considerations in § 2 indicate that similarity based on (u_K, η) can satisfy the Kármán–Howarth equation even when Re_λ is finite provided r is sufficiently small. Equally, the Kármán–Howarth equation admits a similarity solution based on (u', L) when r is sufficiently large. It is therefore reasonable to assume that there are similarity solutions

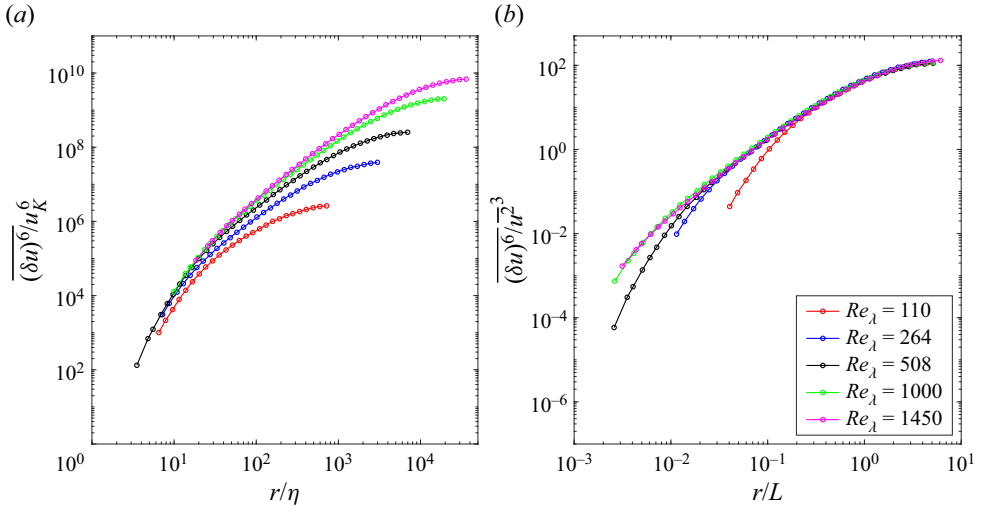

Figure 9. Effect of Re_λ on the distributions of $\overline{(\delta u)^6}$ in grid turbulence. Panels (a,b) are normalized by (u_K, η) and (u', L), respectively. These data are reproduced from Kaminsky *et al.* (2020).

of the form

$$\frac{\overline{(\delta u)^2}}{u_K^2} = f_1\left(\frac{r}{\eta}\right), \tag{4.1}$$

$$\frac{\overline{(\delta u)^2}}{\overline{u^2}} = f_2\left(\frac{r}{L}\right), \tag{4.2}$$

for sufficiently small and large r, respectively. As Re_λ increases, the range of r/η and r/L over which (4.1) and (4.2) are valid also increases (figure 6). The expectation that these ranges must eventually overlap over the inertial range is highly plausible (see Gamard and George's discussion of the overlap in the spectra of u, when normalized by (u_K, η) and (u', L) Gamard & George 2000), especially as $Re_\lambda \to \infty$. Note that we are dealing with the same distributions of $\overline{(\delta u)^2}$, after subjecting it to two different types of normalization. Matching (4.1) with (4.2) requires that

$$u_K^2 f_1\left(\frac{r}{\eta}\right) = \overline{u^2} f_2\left(\frac{r}{L}\right). \tag{4.3}$$

If it is further assumed that, in the inertial range, $f_1(r/\eta)$ exhibits a power-law form, *viz.*

$$f_1\left(\frac{r}{\eta}\right) \sim \left(\frac{r}{\eta}\right)^\alpha, \tag{4.4}$$

then

$$f_2\left(\frac{r}{L}\right) \sim \frac{u_K^2}{\overline{u^2}}\left(\frac{L}{\eta}\right)^\alpha \left(\frac{r}{L}\right)^\alpha. \tag{4.5}$$

For isotropic turbulence, $u_K^2/\overline{u^2} = 15^{1/2}/Re_\lambda$ and $L/\eta = Re_\lambda^{3/2}/15^{3/4}$ if $C_\epsilon = 1$. The plots in figure 6 show that (4.1) and (4.2) are closely satisfied for significant ranges of r/η and r/L. In particular, at the two largest values of Re_λ, the upper value of r/η exceeds

50 whilst the lower value of r/L lies below 0.01. This implies that an overlap region is starting to conform with the expected limits of the inertial range, i.e. $\eta \ll r \ll L$. The Reynolds number independence displayed by figure 6 for $r/\eta \lesssim 50$ and $r/L \gtrsim 0.01$ is expected to be approached in the overlap region. As discussed in §§ 1 and 2, the two scalings should become interchangeable as $Re_\lambda \to \infty$ so that the inertial range should also be independent of Re_λ. The formulation (4.5) or $f_2 \sim Re_\lambda^{3/2\alpha-1}(r/L)^\alpha$ is independent of Re_λ when $3/2\alpha - 1 = 0$, i.e. when $\alpha = 2/3$, which corresponds to the K41 prediction. This result was also derived by Lundgren (2002) from the Kármán–Howarth equation using matched asymptotic expansions when $Re_\lambda \to \infty$. A similar result was derived earlier by Gamard & George (2000) in the context of the u spectrum; the approach adopted in this paper is consistent with the asymptotic invariance principle and the methodology of near-asymptotics, introduced by George (1989, 1994). The previous approach for $\overline{(\delta u)^2}$ can be extended to $\overline{(\delta u)^n}$ (see for example Djenidi *et al.* 2019).

Figures 7–9 indicate that the dual scaling applies to $\overline{(\delta u)^3}$, $\overline{(\delta u)^4}$ and $\overline{(\delta u)^6}$. One would expect that, in general, the dual scaling will also apply to $\overline{(\delta u)^n}$, if the probability distribution function (p.d.f.) of δu complies with the two types of normalization. For simplicity, we next focus on a parametrized form of $\overline{(\delta u)^n}$ (Dhruva 2000; Kurien & Sreenivasan 2000), *viz.*

$$\frac{\overline{(\delta u)^n}}{u_K^n} = \frac{1}{15^{n/2}} F_n \frac{\left(\dfrac{r}{\eta}\right)^n \left(1 + D_n\left(\dfrac{r}{L}\right)\right)^{2C_n - n}}{\left(1 + B_n\left(\dfrac{r}{\eta}\right)^2\right)^{C_n}}, \tag{4.6}$$

where B_n, C_n, D_n and F_n ($\equiv \overline{(\partial u/\partial x)^n}/\overline{(\partial u/\partial x)^2}^{n/2}$) are constants. Note that, for $n > 2$, F_n is only expected to approach a constant value at increasingly larger values of Re_λ as n increases. An earlier version of (4.6), without the large-scale term, *viz.* $(1 + D_n(r/L))^{2C_n - n}$, was proposed by Stolovitzky, Sreenivasan & Juneja (1993) who tested it against laboratory boundary layer data for a moderate Reynolds number ($Re_\lambda \approx 200$). The stated objective was to obtain reliable estimates of the scaling exponents (i.e. C_n). One can however query this objective given that the power-law behaviour of $\overline{(\delta u)^n}$ is rigorous only when the inertial range is established, i.e. $Re_\lambda \to \infty$. As will be shown later, 'ζ_n' for $\overline{(\delta u)^n}$ cannot be defined even at the largest Re_λ (≈ 1500) for the present grid turbulence data; this is not surprising since the 4/5 law has yet to be established (see figure 12*a* later). Dhruva (2000) found that (4.6) provided a good fit to atmospheric surface layer data for $\overline{(\delta u)^2}$, $\overline{(\delta u)^4}$ and $\overline{(\delta u)^6}$ over the complete range of r. Our main interest is that (4.6) should represent as adequate a fit as possible to the experimental data for $\overline{(\delta u)^n}$ irrespectively of n and Re_λ. In particular, the constants in (4.6) should satisfy the asymptotic case ($Re_\lambda \to \infty$). This is really the context in which (4.6) was used by Antonia & Burattini (2006) and Antonia *et al.* (2019) with $n = 2$. In other words, we shall not use (4.6) to estimate C_n for different values of Re_λ, as was done, for example, by Stolovitzky *et al.* (1993). When Re_λ is finite, at least at $Re_\lambda \sim 10^3$, (4.6) does not reduce to a simple power-law form ($\sim r^\alpha$) in the scaling range in various turbulent flows such as the stationary forced periodic box turbulence and along the axes of axisymmetric and plane jets (Tang *et al.* 2017).

Equation (4.6) should be interpreted as a composite model for $\overline{(\delta u)^n}$, which satisfies the dual scaling at small and large r. In particular, in the inertial range ($\eta \ll r \ll L$), (4.6)

reduces to

$$\frac{\overline{(\delta u)^n}}{u_K^n} = \frac{1}{15^{n/2}} F_n B_n^{-C_n} \left(\frac{r}{\eta}\right)^{n-2C_n}. \tag{4.7}$$

Using the isotropic relations $L/\eta = C_\epsilon 15^{-3/4} Re_\lambda^{3/2}$ and $\overline{u^2}/u_K^2 = Re_\lambda/15^{1/2}$, we have

$$\frac{\overline{(\delta u)^n}}{\overline{u^2}^{n/2}} = \frac{15^{n/4} Re_\lambda^{3/2(n-2C_n)}}{15^{n/2} Re_\lambda^{n/2}} F_n B_n^{-C_n} \left(\frac{r}{L}\right)^{n-2C_n} C_\varepsilon^{n-2C_n} 15^{-3/4(n-2C_n)}. \tag{4.8}$$

Note that (4.8) is the generalization of (4.5) to $\overline{(\delta u)^n}$. It is also the starting point of nearly all intermittency models, *viz.* $\overline{(\delta u)^n}/u'^n \sim (r/L)^{\zeta_n}$, with a prefactor that is independent of Re_λ but possibly dependent on the macrostructure of the flow. We underline that (4.8) is equivalent to (4.7) since only a transformation of variables has been applied. If (4.8) is Re_λ-independent, we immediately obtain

$$\tfrac{3}{2}(n - 2C_n) - n/2 = 0, \tag{4.9}$$

which leads to

$$C_n = n/3. \tag{4.10}$$

We will use this value of C_n in (4.6) in the next section. Substituting $C_n = n/3$ into (4.8), we can obtain

$$\frac{\overline{(\delta u)^n}}{\overline{u^2}^{n/2}} = \frac{1}{15^{n/2}} F_n B_n^{-C_n} \left(\frac{r}{L}\right)^{n-2C_n} C_\varepsilon^{n-2C_n}. \tag{4.11}$$

Note that (4.7) and (4.11) are identical if $C_\varepsilon = 1$. The use of $C_n = n/3$ in (4.6) is fully justifiable since (4.6) should comply with complete similarity, i.e. similarity at all values of r/η (or r/L) as $Re_\lambda \to \infty$. For finite values of Re_λ, (4.6) should describe the incomplete similarity inherent in the dual scaling scheme (this will be illustrated in figures 18–21). For $n = 2$, (4.6) was, as noted earlier, used previously and shown to describe adequately the dependence of $\overline{(\delta u)^2}$ on Re_λ in various flows.

It is worth mentioning that, as $r \to \infty$, (4.6) is proportional to $Re_\lambda^{n/2}$ after taking $C_n = n/3$ and using the relation $L/\eta = C_\epsilon 15^{-3/4} Re_\lambda^{3/2}$. This is consistent with the limiting values as $r \to \infty$ for $n = 2, 4$ and 6 (see (3.1), (3.7) and (3.10) of Pearson & Antonia 2001).

5. Comparison between (4.6) and experimental data

Figures 10, 11(*a*)–14(*a*) show a comparison between the experimental data in figures 3, 6(*a*)–9(*a*) and (4.6). Note that we have used $C_n = n/3$; the values for B_n, C_ϵ, D_n and F_n are listed in tables 2 and 3. It is worth mentioning that $B_2 = 0.0056$ and $F_2 = 1$ lead to a Kolmogorov constant for $\overline{(\delta u)^2}$ of $A_2 = 2.11$. Also, $B_3 = 0.0114$ and $-F_3 = 0.53$ lead to a Kolmogorov constant for $\overline{(\delta u)^3}$ of $A_3 = 4/5$. The magnitudes of F_3, F_4 and F_6 used in (4.6) are consistent with the available data in grid turbulence and along the axis of the plane jet (see figure 16 later). The magnitude of C_ϵ $(= 0.8)$ is consistent with the VDTT data at large Re_λ (figure 2). Here, D_2 and D_3 are selected so that (4.6) fits the data for $\overline{(\delta u)^2}/u_K^2$ and $\overline{(\delta u)^3}/u_K^3$ reasonably well at all Re_λ. The magnitudes of D_4 and B_4 are determined by trial and error until (4.6) fits the data for $\overline{(\delta u)^4}/u_K^4$ at all Re_λ; the magnitudes of D_6 and B_6 are determined in the same way. It should be pointed

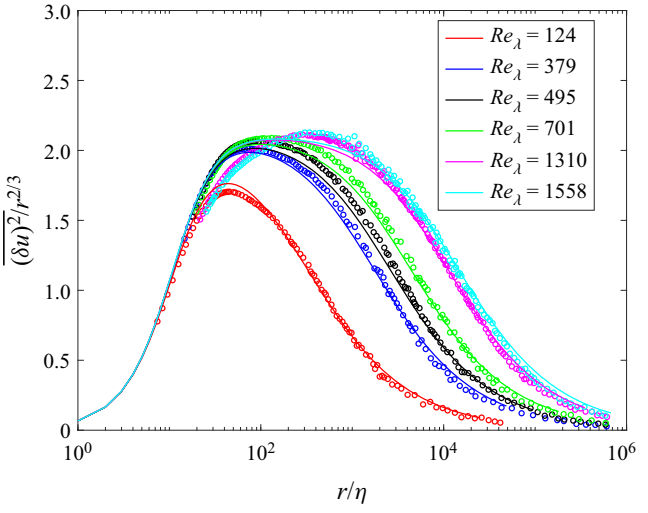

Figure 10. Distributions of $\overline{(\delta u)^2}/(\bar{\epsilon} r)^{2/3}$ based on (4.6) at $Re_\lambda = 124$, 379, 495, 701, 1310 and 1558. Symbols with the same colour correspond to the data of Bodenschatz *et al.* (2014) shown in figure 3.

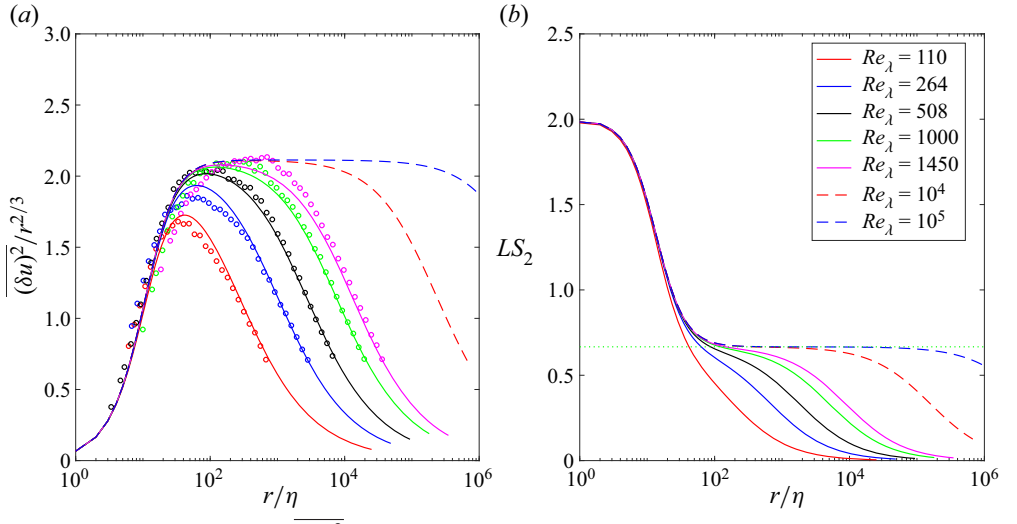

Figure 11. (*a*) Distributions of $\overline{(\delta u)^2}/(\bar{\epsilon} r)^{2/3}$ based on (4.6) at $Re_\lambda = 110$, 264, 508, 1000, 1450, 10^4 and 10^5. Symbols with the same colour are the corresponding grid turbulence data, reproduced from figure 6(*a*). (*b*) Local slope ($LS_2 = \mathrm{d}\log(\overline{(\delta u)^2})/\mathrm{d}\log r$). Dashed horizontal line, 2/3.

out that all the constants B_n, C_n, D_n and F_n are Re_λ-independent except for F_4 in the range $Re_\lambda < 1000$ and for F_6 in the range $Re_\lambda < 1450$. Here, $F_4 = 10$ for $Re_\lambda \geq 1000$ and $B_4 = 0.011$ lead to a Kolmogorov constant for $\overline{(\delta u)^4}$ of $A_4 = 18.18$. Also, $F_6 = 440$ for $Re_\lambda \geq 1450$ and $B_6 = 0.0178$ lead to a Kolmogorov constant for $\overline{(\delta u)^6}$ of $A_6 = 413.33$. In particular, we can obtain two ratios: $A_4/A_2^2 = 4.1$ and $A_6/A_2^3 = 43.7$. Their magnitudes are consistent with the predictions of Qian (2000) who used a non-Gaussian p.d.f. of δu to obtain $A_4/A_2^2 = 4.1$–5.4 and $A_6/A_2^3 = 37.4$–69.0. Here, the main objective of using (4.6), with the above magnitudes for B_n, C_n, D_n and F_n in grid turbulence, is to describe

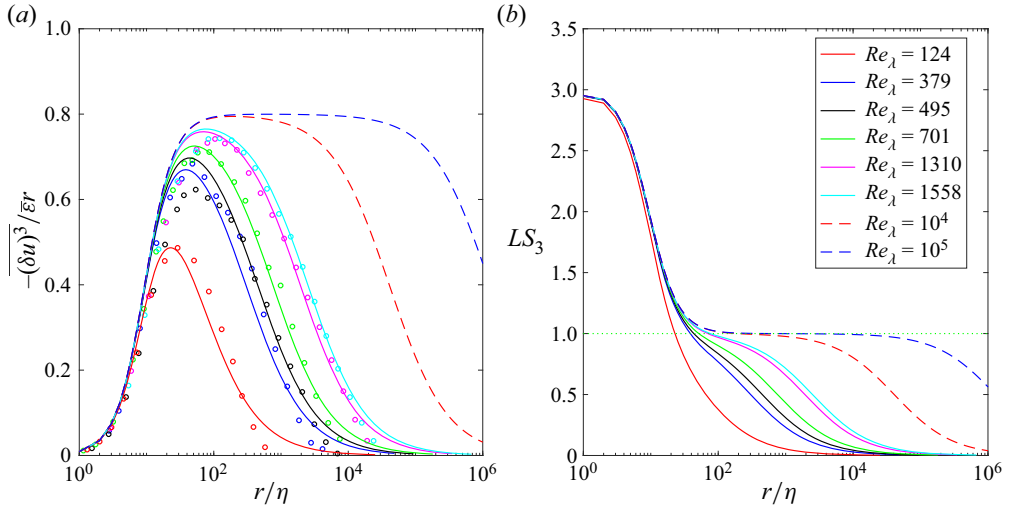

Figure 12. (*a*) Distributions of $-\overline{(\delta u)^3}/\bar{\epsilon}r$ based on (4.6) at $Re_\lambda = 117$, 352, 535, 679, 1323, 1548, 10^4 and 10^5. Symbols with the same colour are the corresponding grid turbulence data, reproduced from figure 7(*a*). (*b*) Local slope ($LS_3 = \mathrm{d}\log(-\overline{(\delta u)^3})/\mathrm{d}\log r$). Dashed horizontal line, 1.

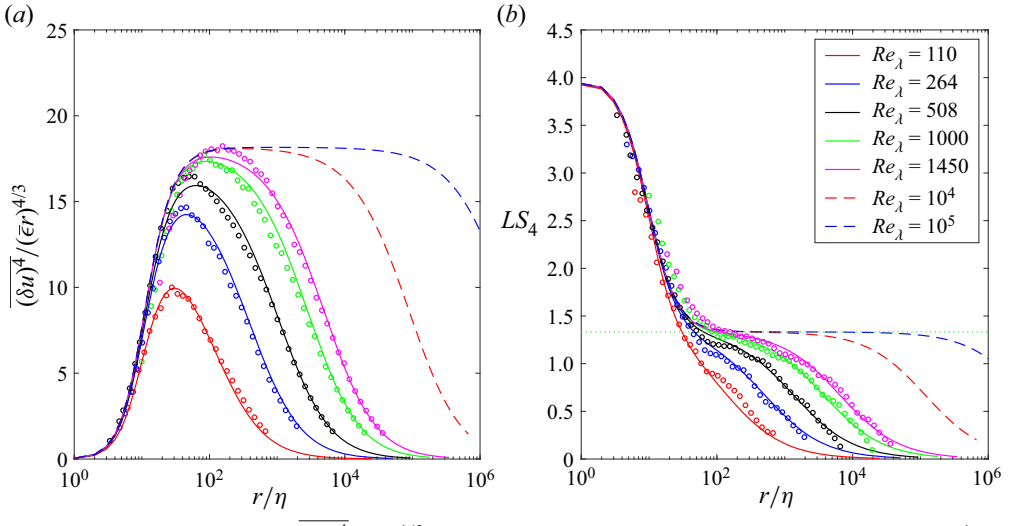

Figure 13. (*a*) Distributions of $\overline{(\delta u)^4}/(\bar{\epsilon}r)^{4/3}$ based on (4.6) at $Re_\lambda = 110$, 264, 508, 1000, 1450, 10^4 and 10^5. Symbols with the same colour are the corresponding grid turbulence data, reproduced from figure 8(*a*). (*b*) Local slope ($LS_4 = \mathrm{d}\log(\overline{(\delta u)^4})/\mathrm{d}\log r$) corresponding to the distributions in (*a*). Dashed horizontal line, 4/3.

the dependence on Re_λ of the available experimental data for $\overline{(\delta u)^n}/u_K^n$ which allows us to extrapolate the $\overline{(\delta u)^n}/u_K^n$ distributions to infinitely large Re_λ. The local slope LS_n ($= \mathrm{d}\log|\overline{(\delta u)^n}|/\mathrm{d}\log r$), based on (4.6), is shown in figures 11(*b*)–14(*b*). Note that the local slope LS_2 of the distributions in figure 10 is similar to that in figure 11(*b*) and thus not shown. We can observe from these figures that the agreement between curves and symbols is satisfied approximately at almost all scales over a significant range of Re_λ, confirming the adequacy of the fit used to emulate the available data for $\overline{(\delta u)^2}$,

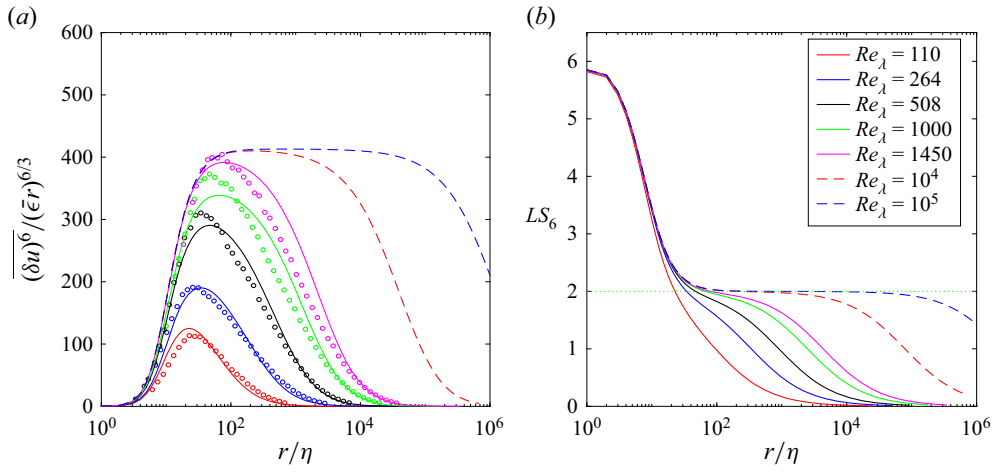

Figure 14. (*a*) Distributions of $\overline{(\delta u)^6}/(\bar{\epsilon}r)^{6/3}$ based on (4.6) at $Re_\lambda = 110$, 264, 508, 1000, 1450, 10^4 and 10^5. Symbols with the same colour are the corresponding grid turbulence data, reproduced from figure 9(*a*). (*b*) Local slope ($LS_6 = \mathrm{d}\log(\overline{(\delta u)^6})/\mathrm{d}\log r$). Dashed horizontal line, 6/3.

C_ϵ	D_2	B_2	F_2	D_4	B_4	D_6	B_6	D_3	B_3	$-F_3$
0.8	0.67	0.0056	1	0.88	0.011	1.33	0.0178	2.58	0.0114	0.53

Table 2. Values of B_n, C_ϵ, D_n, F_2 and F_3 used in figures 10–21. Note that the magnitudes of F_3 are compared with data in grid turbulence and along the axis of the plane jet in figure 16.

Re_λ	110	264	508	1000	$\geq$1450
F_4	8.1	9.3	9.6	10	10
F_6	124	270	360	360	440

Table 3. Values of F_4 and F_6 used in figures 13–17 and 20–21. Note that the magnitudes of F_4 and F_6 are compared with data in grid turbulence and along the axis of the plane jet in figure 16.

$\overline{(\delta u)^3}$, $\overline{(\delta u)^4}$ and $\overline{(\delta u)^6}$. It should be pointed out that the agreement between the model and the data for some of the distributions at large Re_λ and at moderate scales is not so good, as seen for example for the distributions of $\overline{(\delta u)^2}/(\bar{\epsilon}r)^{2/3}$ at $Re_\lambda = 1310$ and 1558 in the range $r/\eta \approx 20$–100, which correspond to the range $k_1\eta \approx 0.06$–0.31 in the energy spectra. We can indeed observe from figure 1(*a*) that the magnitude of the Kolmogorov-normalized energy spectra in the range $k_1\eta \approx 0.06$–0.31 at $Re_\lambda = 1310$ and 1558 is smaller than that for all the other distributions, including those of Bodenschatz *et al.* (2014) at $Re_\lambda = 124$, 379, 495 and 701 and Larssen & Devenport (2011) at $Re_\lambda = 124$ and 1360. This corresponds to $\overline{(\delta u)^2}/(\bar{\epsilon}r)^{2/3}$ being underestimated at $Re_\lambda = 1310$ and 1558 in the range $r/\eta \approx 20$–100 which is most likely due to the measurement uncertainty. We next use the Kármán–Howarth equation (2.1) to further examine the data of Bodenschatz *et al.* (2014). The distributions of $-\overline{(\delta u)^3}/\bar{\epsilon}r$ in figure 15 are calculated using (2.1) and (4.6) with $n = 2$ at $Re_\lambda = 117$, 352, 535, 679, 1323 and 1548. We emphasize that using

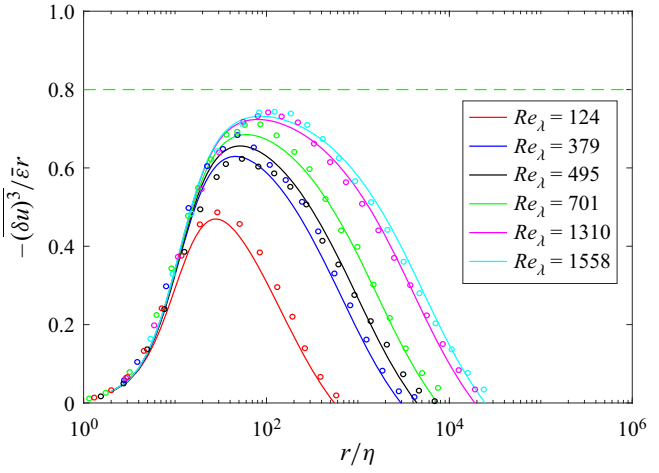

Figure 15. Analytical predictions of $-\overline{(\delta u)^3}/\bar{\epsilon}r$ (curves) based on (2.1) and (4.6) with $n = 2$ at $Re_\lambda = 117$, 352, 535, 679, 1323 and 1548. The details of how the integral term in (2.1), i.e. $I_u(r)$ term, was calculated are discussed elsewhere (see for example (4.9) of Tang *et al.* (2017) where the power-law decay rate for $\overline{u^2}$, *viz.* $\overline{u^2} \sim x^n$ with $n \approx -1.2$ (Sinhuber *et al.* 2015), was used here). Symbols with the same colour are the corresponding grid turbulence data, reproduced from figure 12(*a*). The dashed horizontal line in each plot corresponds to the value of 4/5.

(4.6) with $n = 2$ is equivalent to using of the experimental data for $\overline{(\delta u)^2}/(\bar{\epsilon}r)^{2/3}$ in figure 10; here we used the former since the calculation of the integral term in (2.1), i.e. $I_u(r)$ term, based on (4.6) with $n = 2$ should be more accurate than that based on the discrete experimental data. Also shown in figure 15 are the grid turbulence data (symbols) at the same Re_λ, reproduced from figure 12(*a*). The agreement between curves and symbols in figure 15 is satisfactory. This agreement not only confirms the fit (i.e. (4.6) with $n = 2$) used to emulate the available data for $\overline{(\delta u)^2}/(\bar{\epsilon}r)^{2/3}$ (figure 10), but also vindicates the choice of M for $\overline{(\delta u)^2}/u_K^2$ in figure 4. Finally, figure 15 further indicates that the magnitude of the model at $Re_\lambda = 1310$ and 1558 in the range $r/\eta \approx 20$–100 being larger than that of the data most likely reflects a measurement uncertainty in the experimental data (figure 10). Correspondingly, the magnitude of the energy spectrum distributions in the range $k_1\eta \approx 0.06$–0.31 at $Re_\lambda = 1310$ and 1558 in figure 1(*a*) being smaller than that of all other distributions also most likely reflects a measurement uncertainty. Further, there is no well-defined plateau for all the experimental data (figures 10, 11*a*–14*a*), even at $Re_\lambda \sim 1500$, underlining the importance of the FRN effect in the context of establishing the inertial range. This effect can be also observed in the LS_n distributions for all the experimental data; as an example, we have included in figure 13(*b*) the local slope LS_4 for the corresponding VDTT grid turbulence data of Kaminsky *et al.* (2020). In particular, LS_3 for $Re_\lambda = 1558$ is far from exhibiting a plateau (figure 12*b*), implying that (1.2) is actually far from being satisfied by the VDTT grid turbulence data, which underlines the absence of an IR. Note that the calculated distributions indicate that a plateau is likely to emerge as Re_λ increases to an infinitely large value. Both the VDTT grid turbulence data and LS_n distributions based on (4.6) in figures 10, 11–14 show an evolution of $\overline{(\delta u)^n}$ and the corresponding local slopes with Re_λ with a slow approach to $n/3$. Such a trend is not only consistent with all the analysis in the present paper, but also consistent with the plane jet data of Tang *et al.* (2017). Finally, we should also stress that the local slopes LS_n are

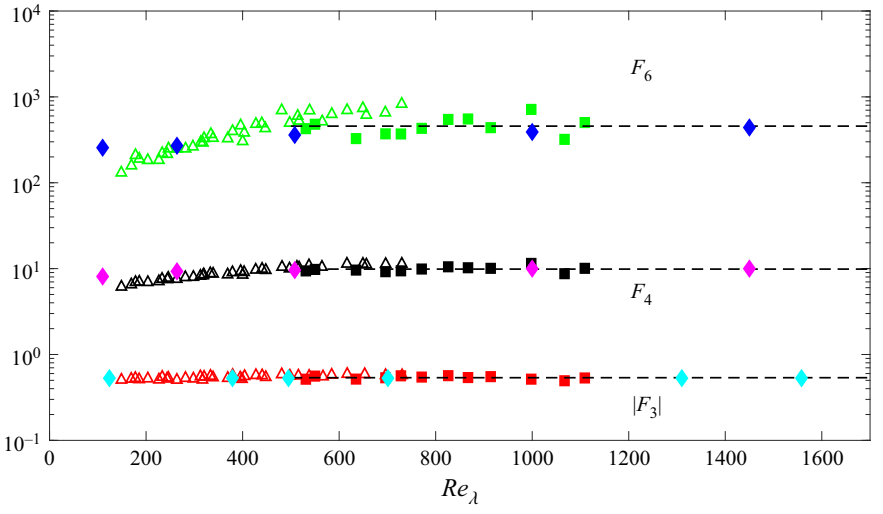

Figure 16. The magnitudes (diamonds) of $|F_3|$, F_4 and F_6 used to plot figures 12–14. For reference, the data along the axis of the plane jet, reproduced from Antonia *et al.* (2017) (triangles), and in grid turbulence, reproduced from Gylfason *et al.* (2004) (squares), are also shown; for the latter, only the laboratory shearless grid turbulence data are shown. The horizontal dashed lines indicate the mean values of each of the plotted quantities for the plane jet data.

not affected by the values of $\bar{\varepsilon}$. Obviously, they are not affected by the choice of the value of M used in replotting the $\overline{(\delta u)^n}/u_K^n$ distributions.

Figures 11–14 indicate that Re_λ may need to be of order 10^5 before an inertial range is established unequivocally. To our knowledge, this should be the first time that plausible evidence has been presented for the approach to the IR based on values of n extending to six. We next quantify, albeit approximately, the values of Re_λ required for an inertial range to be established for $\overline{(\delta u)^n}$. Figure 17 shows the range of r/λ over which the distributions, based on (4.6), of $\overline{(\delta u)^2}/(\bar{\epsilon}r)^{2/3}$, $-\overline{(\delta u)^3}/\bar{\epsilon}r$, $\overline{(\delta u)^4}/(\bar{\epsilon}r)^{4/3}$ and $\overline{(\delta u)^6}/(\bar{\epsilon}r)^{6/3}$ depart from 2.11, 4/5, 18.16 and 413 (these values correspond to the plateaus at $Re_\lambda = 10^5$ in figures 11(a)–14(a), respectively, by no more than 2.5 %. It should be pointed out that another possibility would be to use $r = \lambda$ as the 'base' line for IR. This is consistent with Obligado & Vassilicos (2019) and Meldi & Vassilicos (2021) who showed, using the eddy damped quasinormal Markovian, that the interscale energy flux is closest to $\bar{\epsilon}$ when r is close to λ while the larger r, compared to λ, the larger the departure from equilibrium in which the interscale energy flux is equal to $\bar{\epsilon}$. This would result in slightly larger values of Re_λ being required to establish the IR. We can observe from figure 17 that, when n is even, the larger n is being required, the slower is the rate at which $C_n = n/3$ is established convincingly. Interestingly, the r/λ range for $\overline{(\delta u)^6}/(\bar{\epsilon}r)^{6/3}$ is close to that for $-\overline{(\delta u)^3}/\bar{\epsilon}r$. Finally, we can observe that $C_2 = 2/3$ is attained at a smaller Re_λ than $C_3 = 1$. This is consistent with the observation of Antonia *et al.* (2019) where a similar model for $\overline{(\delta u)^2}$ with a slightly different constant ($B_2 = 0.0061$) was used and $\overline{(\delta u)^3}/(\bar{\epsilon}r)$ was calculated from the Kármán–Howarth equation.

It is of interest to examine the dual scaling using (4.6) at large Re_λ. Figures 18–21 show the distributions of $\overline{(\delta u)^n}$ ($n = 2, 3, 4, 6$) normalized by (u_K, η) and (u', L) in grid turbulence at $Re_\lambda = 1600$–10^5. In conformity with the observation based on figures 6–9,

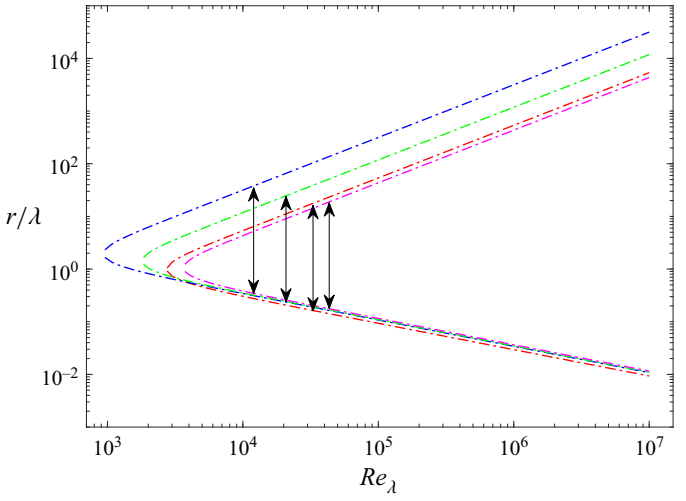

Figure 17. The range of r/λ over which $\overline{(\delta u)^2}/(\bar{\epsilon}r)^{2/3}$ (blue line), $\overline{(\delta u)^3}/(\bar{\epsilon}r)$ (red line), $\overline{(\delta u)^4}/(\bar{\epsilon}r)^{4/3}$ (green line) and $\overline{(\delta u)^6}/(\bar{\epsilon}r)^{6/3}$ (pink line) depart from 2.11, 4/5, 18.16 and 413 (these values correspond to the plateaus at $Re_\lambda = 10^5$ in figures 11*a*–14*a*), respectively, by no more than 2.5 %; they are calculated based on (4.6), using $C_n = n/3$ and the constants for B_n, C_ϵ/D_n and F_n in table 2. The locations of the vertical arrows give an approximate indication of the values of Re_λ needed to attain an IR, of two decades in extent, for $\overline{(\delta u)^2}/(\bar{\epsilon}r)^{2/3}$ (blue arrow), $\overline{(\delta u)^3}/(\bar{\epsilon}r)$ (red arrow), $\overline{(\delta u)^4}/(\bar{\epsilon}r)^{4/3}$ (green arrow) and $\overline{(\delta u)^6}/(\bar{\epsilon}r)^{6/3}$ (pink arrow).

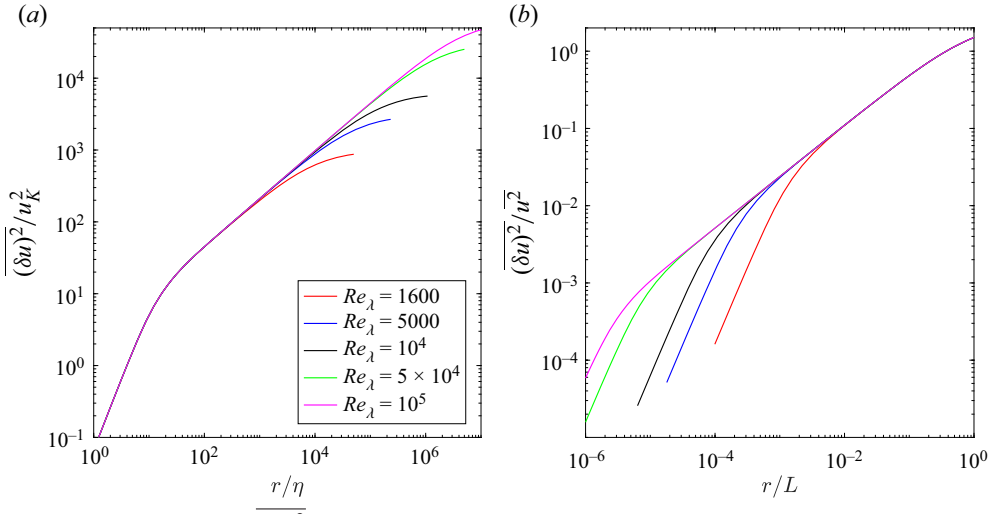

Figure 18. Distributions of $\overline{(\delta u)^2}$ at large Re_λ in grid turbulence. Panels (*a*,*b*) are normalized by (u_K, η) and (u', L), respectively.

the scaling based on (u', L) extends to increasingly smaller values of r/L while the scaling based on (u_K, η) extends to increasingly larger values of r/η as Re_λ increases. In particular, at the two largest values of Re_λ, the upper value of r/η exceeds 10^4 for all $\overline{(\delta u)^n}$ whilst the lower value of r/L lies below 5×10^{-4}. Taking $Re_\lambda = 2 \times 10^4$ and using the isotropic relation $L/\eta = C_\epsilon(Re_\lambda^{3/2}/15^{3/4})$ with $C_\epsilon = 0.8$, we can estimate that the overlap region is given by $10^2 \lesssim r/\eta \lesssim 10^4$. Namely, a distinct range of overlap between the (u', L) and (u_K, η) scalings can be observed at $Re_\lambda = 2 \times 10^4$, suggesting the onset of an inertial

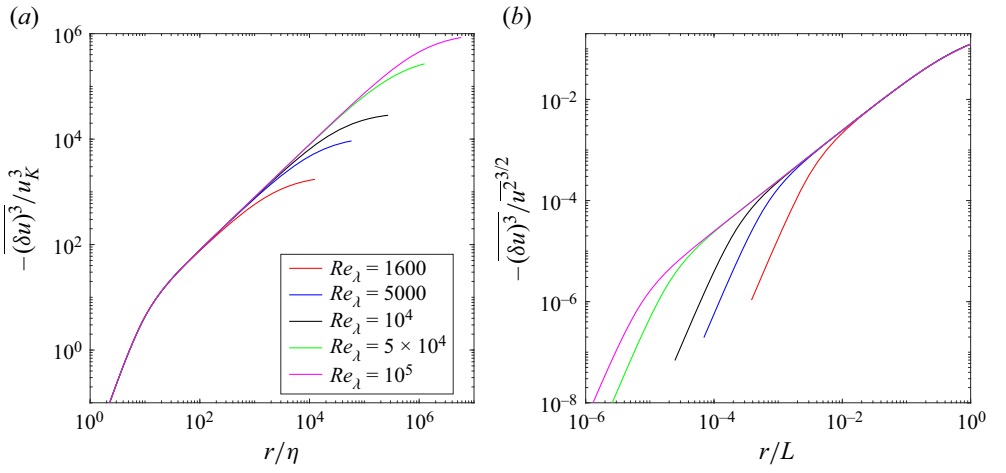

Figure 19. Distributions of $-\overline{(\delta u)^3}$ at large Re_λ in grid turbulence. Panels (a,b) are normalized by (u_K, η) and (u', L), respectively.

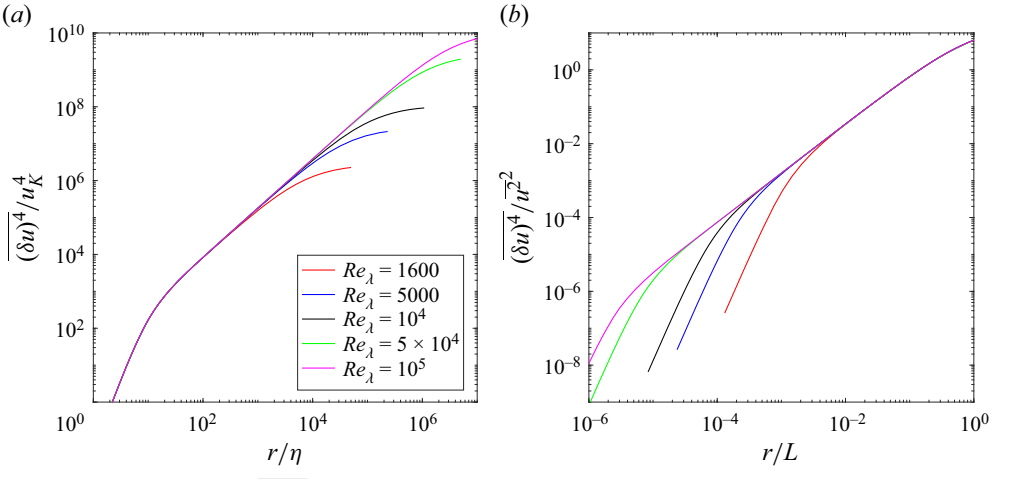

Figure 20. Distributions of $\overline{(\delta u)^4}$ at large Re_λ in grid turbulence. Panels (a,b) are normalized by (u_K, η) and (u', L), respectively.

range for $\overline{(\delta u)^n}$ ($n = 2, 3, 4, 6$) (see also figure 17). These results further confirm that the dual scaling applies to $\overline{(\delta u)^n}$ and an overlap range begins to emerge when $Re_\lambda > 10^4$.

6. Conclusions

A dual scaling analysis has been carried out in the context of the Kármán–Howarth equation, or transport equation for $\overline{(\delta u)^2}$, for grid turbulence. When the effect of the large-scale term is neglected, the scaling (u_K, η) should be effective, even at moderate Re_λ, since the two dimensionless parameters in (2.6a,b) are universal. Also, when the viscous term is neglected, the scaling (u', L) should be also tenable since both $\bar{\varepsilon}L/u'^3$ and $(1/u')(\mathrm{d}L/\mathrm{d}x)$ should approach constant values as Re_λ increases. At finite Re_λ, the dual scaling approach is consistent with incomplete similarity. As $Re_\lambda \to \infty$, it becomes compatible with complete similarity. The dual scaling approach is subsequently tested in

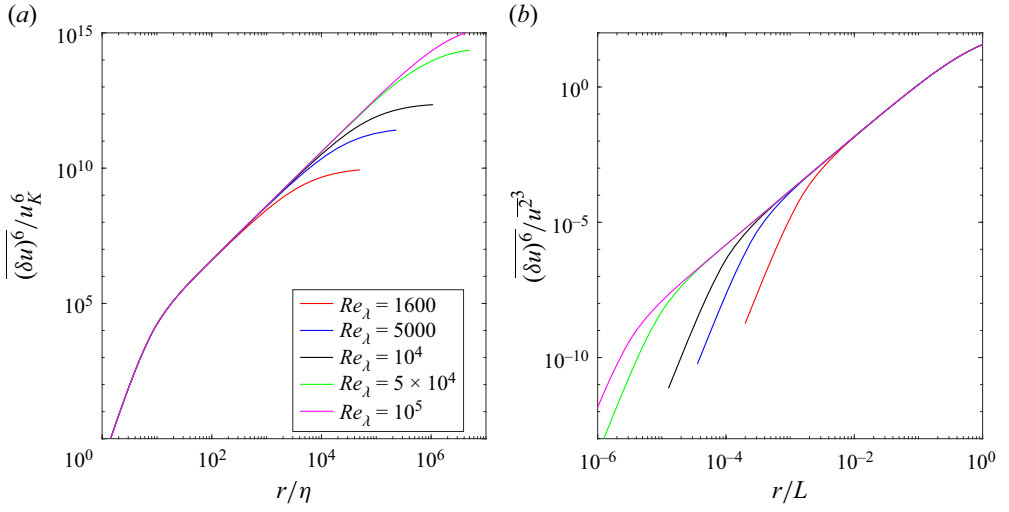

Figure 21. Distributions of $\overline{(\delta u)^6}$ at large Re_λ in grid turbulence. Panels (a,b) are normalized by (u_K, η) and (u', L), respectively.

the context of $\overline{(\delta u)^n}$ ($n \geq 2$) using the VDTT grid turbulence data at $Re_\lambda = 110$–1558 (figures 6–9). It is found that the scaling based on (u', L) extends to increasingly smaller values of r/L as Re_λ increases. Further, the scaling based on (u_K, η) extends to increasingly larger values of r/η as Re_λ increases. These observations are consistent with the dual scaling analysis in the context of the Kármán–Howarth equation. More importantly, the inference from these observations is that both scalings should eventually overlap, as Re_λ increases further, and conform with the power-law relation $\overline{(\delta u)^n} \sim r^{n/3}$ as $Re_\lambda \to \infty$. The extent of the overlap should become significant as $Re_\lambda \to \infty$ since the KH equation has been shown (George 1992; Speziale & Bernard 1992; Djenidi & Antonia 2015; Djenidi *et al.* 2019) to admit a similarity solution based on a single set of scales; in this case, (u', L) can be interchanged with (u_K, η).

An empirical model for $\overline{(\delta u)^n}$ ($n = 2, 3, 4, 6$), i.e. (4.6), has been compared with the VDTT grid turbulence data (figures 10, 11*a*–14*a*). The model, which is consistent with $\overline{(\delta u)^n} \sim r^{n/3}$ as $Re_\lambda \to \infty$, is in reasonable accord with the data for values of Re_λ up to approximately 1500, thus allowing extrapolation of the model-based results to larger values of Re_λ. The major conclusions with respect to the comparison and extrapolation can be summarized as follows.

(i) There is strictly no power-law range for the experimental data of $\overline{(\delta u)^n}$, even at $Re_\lambda \sim 1500$. It is evident that for all the values of n considered here, the local slope LS_n continues to evolve with Re_λ (figures 11*b*–14*b*) and begins to exhibit a small plateau only when Re_λ exceeds 10^4. An important inference from this trend is that the VDTT data, like the spectral data of Mydlarski & Warhaft (1996) and subsequent analysis by Gamard & George (2000), are consistent with (1.3) and do not support (1.4) when $\zeta_n \neq n/3$.

(ii) The FRN effect may differ between even- and odd-order moments of δu. Different values of Re_λ may therefore be required, between even- and odd-order moments of δu, for compliance with $\zeta_n = n/3$. This effect, which, as noted in item (i), is evident in the VDTT data, has, by and large, been either ignored or underestimated in the literature. The approach to $\zeta_n = n/3$ is consistent with the inequality constraint

discussed by Djenidi *et al.* (2023) and with the dual scaling approach outlined in this paper.

(iii) The dual scaling can be used to adequately describe $\overline{(\delta u)^n}$. A larger Re_λ results in wider r/η and r/L ranges over which the scalings (u_K, η) and (u', L) are tenable. We should stress that the empirical model for $\overline{(\delta u)^n}$, i.e. (4.6), does not provide a perfect description of the data. However, it adequately describes the dependence, irrespectively of n, on Re_λ. Furthermore, it fully complies with the dual scaling methodology and satisfies the limiting behaviour of $\overline{(\delta u)^n}$ as $r \to \eta$ and $r \to L$. We should also point out that (4.6) reflects the strongly non-Gaussian character of the small scale turbulence when $r \to 0$ and they transition to quasi Gaussian properties when r exceeds L. The compliance of (4.6) with $\overline{(\delta u)^n} \sim r^{n/3}$ when $Re_\lambda \to \infty$ is consistent with the observation by Qian (2000) and Qian (2001) who used a non-Gaussian p.d.f. of δu with stretched exponential tails together with a 'quasi-closure' scheme to show that $\overline{(\delta u)^n} \sim r^{n/3}$ as $Re_\lambda \to \infty$.

Funding. This research was supported by the National Natural Science Foundation of China (project no. 91952109), Guangdong Basic and Applied Basic Research Foundation (project no. 2023B1515020069) and Shenzhen Science and Technology Program (project nos. RCYX20210706092046085 and GXWD20220817171516009).

Declaration of interests. The authors report no conflict of interest.

Author ORCIDs.
S.L. Tang https://orcid.org/0000-0001-6379-8505;
L. Djenidi https://orcid.org/0000-0001-8614-3595.

References

Antonia, R.A., Tang, S.L., Djenidi, L. & Zhou, Y. 2019 Finite Reynolds number effect and the 4/5 law. *Phys. Rev. Fluids* **4** (8), 084602.

Antonia, R.A. & Burattini, P. 2006 Approach to the 4/5 law in homogeneous isotropic turbulence. *J. Fluid Mech.* **550**, 175–184.

Antonia, R.A., Djenidi, L. & Danaila, L. 2014 Collapse of the turbulent dissipation range on Kolmogorov scales. *Phys. Fluids* **26**, 045105.

Antonia, R.A., Djenidi, L., Danaila, L. & Tang, S.L. 2017 Small scale turbulence and the finite Reynolds number effect. *Phys. Fluids* **29** (2), 020715.

Antonia, R.A., Satyaprakash, B.R. & Hussain, A.K.M.F. 1980 Measurements of dissipation rate and some other characteristics of turbulent plane and circular jets. *Phys. Fluids* **23**, 695–700.

Antonia, R.A., Smalley, R.J., Zhou, T., Anselmet, F. & Danaila, L. 2003 Similarity of energy structure functions in decaying homogeneous isotropic turbulence. *J. Fluid Mech.* **487**, 245–269.

Antonia, R.A., Zhou, T., Danaila, L. & Anselmet, F. 2000 Streamwise inhomogeneity of decaying grid turbulence. *Phys. Fluids* **12**, 3086.

Antonia, R.A., Zhou, T. & Zhu, Y. 1998 Three-component vorticity measurements in a turbulent grid flow. *J. Fluid Mech.* **374**, 29–57.

Barenblatt, G.I. & Chorin, A.J. 1998 New perspectives in turbulence: scaling laws, asymptotics, and intermittency. *SIAM Rev.* **40** (2), 265–291.

Barenblatt, G.I. & Goldenfeld, N. 1995 Does fully developed turbulence exist? Reynolds number independence versus asymptotic covariance. *Phys. Fluids* **7**, 3078–3082.

Benzi, R., Ciliberto, S., Tripiccione, R., Baudet, C., Massaioli, F. & Succi, S. 1993 Extended self-similarity in turbulent flows. *Phys. Rev.* E **48**, 29–32.

Birnir, B. 2019 The turbulence problem. *Nonlinear Stud.* **26**, 767–781.

Bodenschatz, E., Bewley, G.P., Nobach, H., Sinhuber, M. & Xu, H. 2014 Variable density turbulence tunnel facility. *Rev. Sci. Instrum.* **85** (9), 093908.

Burattini, P., Antonia, R.A. & Danaila, L. 2005*a* Similarity in the far field of a turbulent round jet. *Phys. Fluids* **17**, 025101.

BURATTINI, P., LAVOIE, P. & ANTONIA, R. 2005*b* On the normalized turbulent energy dissipation rate. *Phys. Fluids* **17**, 98103.

CAO, N., CHEN, S. & DOOLEN, G.D. 1999 Statistics and structures of pressure in isotropic turbulence. *Phys. Fluids* **11**, 2235–2250.

COMTE-BELLOT, G. & CORRSIN, S. 1966 The use of a contraction to improve the isotropy of grid-generated turbulence. *J. Fluid Mech.* **25**, 657–682.

COMTE-BELLOT, G. & CORRSIN, S. 1971 Simple Eulerian time correlation of full-and narrow-band velocity signals in grid-generated, 'isotropic' turbulence. *J. Fluid Mech.* **48** (2), 273–337.

DANAILA, L., ANSELMET, F. & ANTONIA, R.A. 2002 An overview of the effect of large-scale inhomogeneities on small-scale turbulence. *Phys. Fluids* **14**, 2475–2482.

DANAILA, L., ANSELMET, F., ZHOU, T. & ANTONIA, R.A. 1999 A generalization of Yaglom's equation which accounts for the large-scale forcing in heated decaying turbulence. *J. Fluid Mech.* **391**, 359–372.

DHRUVA, B. 2000 An Experimental Study of High Reynolds Number Turbulence in the Atmosphere. PhD thesis, Yale University.

DICKEY, T.D. & MELLOR, G.L. 1979 The Kolmogoroff $r^2/3$ law. *Phys. Fluids* **22**, 1029–1032.

DJENIDI, L., ANTONIA, R.A. & TANG, S.L. 2019 Scale invariance in finite Reynolds number homogeneous isotropic turbulence. *J. Fluid Mech.* **864**, 244–272.

DJENIDI, L. & ANTONIA, R.A. 2012 A spectral chart method for estimating the mean turbulent kinetic energy dissipation rate. *Exp. Fluids* **53**, 1005–1013.

DJENIDI, L. & ANTONIA, R.A. 2015 A general self-preservation analysis for decaying homogeneous isotropic turbulence. *J. Fluid Mech.* **773**, 345–365.

DJENIDI, L., ANTONIA, R.A. & TANG, S.L. 2022 Scaling of velocity structure functions in isotropic turbulence. In *Proceedings 23rd Australasian Fluid Mechanics Conference, Sydney, Australia*.

DJENIDI, L., ANTONIA, R.A. & TANG, S.L. 2023 Scaling of turbulent velocity structure functions: plausibility constraints. *J. Fluid Mech.* **965**, A14.

DONZIS, D.A., SREENIVASAN, K.R. & YEUNG, P.K. 2005 Scalar dissipation rate and dissipative anomaly in isotropic turbulence. *J. Fluid Mech.* **532**, 199–216.

GAMARD, S. & GEORGE, W.K. 2000 Reynolds number dependence of energy spectra in the overlap region of isotropic turbulence. *Flow Turbul. Combust.* **63**, 443–477.

GEORGE, W.K. 1989 The self-preservation of turbulent flows and its relation to initial conditions and coherent structures. In *Advances in Turbulence* (ed. W.K. George & R. Arndt), pp. 39–73. Hemisphere.

GEORGE, W.K. 1992 The decay of homogeneous isotropic turbulence. *Phys. Fluids* **4**, 1492–1509.

GEORGE, W.K. 1994 Some new ideas for similarity of turbulent shear flows. In *Proceedings of Turbulence, Heat and Mass Transfer Symposium Lisbon, Portugal* (ed. K. Hanjalic & J. Pereira), pp. 24–49. Begell House.

GOTOH, T., FUKAYAMA, D. & NAKANO, T. 2002 Velocity field statistics in homogeneous steady turbulence obtained using a high-resolution direct numerical simulation. *Phys. Fluids* **14**, 1065–1081.

GYLFASON, A., AYYALASOMAYAJULA, S. & WARHAFT, Z. 2004 Intermittency, pressure and acceleration statistics from hot-wire measurements in wind-tunnel turbulence. *J. Fluid Mech.* **501**, 213–229.

HE, G.W., JIN, G.D. & YANG, Y. 2017 Space–time correlations and dynamic coupling in turbulent flows. *Annu. Rev. Fluid Mech.* **49**, 51–70.

HILL, R.J. 2001 Equations relating structure functions of all orders. *J. Fluid Mech.* **434**, 379–388.

ISHIHARA, T., GOTOH, T. & KANEDA, Y. 2009 Study of high-Reynolds number isotropic turbulence by direct numerical simulation. *Annu. Rev. Fluid Mech.* **41**, 165–80.

ISHIHARA, T. & KANEDA, Y. 2002 High resolution DNS of incompressible homogeneous forced turbulence: time dependence of the statistics. In *Proceedings of the International Workshop on Statistical Theories and Computational Approaches to Turbulence* (ed. Y. Kaneda & T. Gotoh), pp. 177–188. Springer.

IYER, K.P., SREENIVASAN, K.R. & YEUNG, P.K. 2020 Scaling exponents saturate in three-dimensional isotropic turbulence. *Phys. Rev. Fluids* **5** (5), 054605.

JIMENEZ, J., WRAY, A.A., SAFFMAN, P.G. & ROGALLO, R.S. 1993 The structure of intense vorticity in isotropic turbulence. *J. Fluid Mech.* **255**, 65–90.

KAMINSKY, J., BIRNIR, B., BEWLEY, G.P. & SINHUBER, M. 2020 Reynolds number dependence of the structure functions in homogeneous turbulence. *J. Nonlinear Sci.* **30** (3), 1081–1114.

VON KÁRMÁN, T. & HOWARTH, L. 1938 On the statistical theory of isotropic turbulence. *Proc. R. Soc. Lond.* A **164**, 192–215.

KOLMOGOROV, A.N. 1941*a* The local structure of turbulence in incompressible viscous fluid for very large Reynolds number. *Dokl. Akad. Nauk SSSR* **30**, 299–303 (see also *Proc. R. Soc. Lond.* A **434**, 9–13).

KOLMOGOROV, A.N. 1941*b* Dissipation of energy in the locally isotropic turbulence. *Dokl. Akad. Nauk SSSR* **32**, 19–21 (see also *Proc. R. Soc. Lond.* A (1991), **434**, 15–17).

KOLMOGOROV, A.N. 1962 A refinement of previous hypotheses concerning the local structure of turbulence in a viscous incompressible fluid at high Reynolds number. *J. Fluid Mech.* **13**, 82–85.
KURIEN, S. & SREENIVASAN, K.R. 2000 Anisotropic scaling contributions to high-order structure functions in high-Reynolds-number turbulence. *Phys. Rev.* E **62**, 2206–2212.
LANDAU, L.D. & LIFSHITZ, E.M. 1987 *Fluid Mechanics: Vol 6 of course of theoretical physics, Second English Edition, Revised*. Pergamon.
LARSSEN, J.V. & DEVENPORT, W.J. 2011 On the generation of large-scale homogeneous turbulence. *Exp. Fluids* **50**, 1207–1223.
LAVOIE, P., DJENIDI, L. & ANTONIA, R.A. 2007 Effects of initial conditions in decaying turbulence generated by passive grids. *J. Fluid Mech.* **585**, 395–420.
LEE, S.K., DJENIDI, L., ANTONIA, R.A. & DANAILA, L. 2013 On the destruction coefficients for slightly heated decaying grid turbulence. *Intl J. Heat Fluid Flow* **43**, 129–136.
LUNDGREN, T.S. 2002 Kolmogorov two-thirds law by matched asymptotic expansion. *Phys. Fluids* **14** (2), 638–642.
LUNDGREN, T.S. 2003 Kolmogorov turbulence by matched asymptotic expansions. *Phys. Fluids* **15** (4), 1074–1081.
MALECOT, Y. 1998 Intermittence en turbulence 3D: statistiques de la vitesse et de la vorticité. PhD thesis, University of Grenoble.
MCCOMB, W.D., YOFFE, S.R., LINKMANN, M.F. & BERERA, A. 2014 Spectral analysis of structure functions and their scaling exponents in forced isotropic turbulence. *Phys. Rev.* E **90** (5), 053010.
MCCOMB, W.D., BERERA, A., YOFFE, S.R. & LINKMANN, M.F. 2015 Energy transfer and dissipation in forced isotropic turbulence. *Phys. Rev.* E **91**, 043013.
MCKEON, B.J. & MORRISON, J.F. 2007 Asymptotic scaling in turbulent pipe flow. *Phil. Trans. R. Soc.* A **365** (1852), 771–787.
MELDI, M., DJENIDI, L. & ANTONIA, R.A. 2021 Sensitivity analysis of the second and third-order velocity structure functions to the Reynolds number in decaying and forced isotropic turbulence using the EDQNM model. *Eur. J. Mech. (B/Fluids)* **88**, 229–242.
MELDI, M. & VASSILICOS, J.C. 2021 Analysis of Lundgren's matched asymptotic expansion approach to the Kármán-Howarth equation using the eddy damped quasi-normal Markovian turbulence closure. *Phys. Rev. Fluids* **6**, 064602.
MI, J., XU, M. & ZHOU, T. 2013 Reynolds number influence on statistical behaviors of turbulence in a circular free jet. *Phys. Fluids* **25**, 075101.
MILLIKAN, C.B. 1939 A critical discussion of turbulent flows in channels and tubes. In *Proceedings of the 5th International Congress on Applied Mechanics* (ed. J.P. Den Hartog & H. Peters), pp. 386–392. Wiley.
MONIN, A.S. & YAGLOM, A.M. 2007 *Statistical Fluid Dynamics*, vol. 2. MIT.
MYDLARSKI, L. & WARHAFT, Z. 1996 On the onset of high-Reynolds-number grid-generated wind tunnel turbulence. *J. Fluid Mech.* **320**, 331–368.
MYDLARSKI, L. & WARHAFT, Z. 1998 Passive scalar statistics in high-Péclet-number grid turbulence. *J. Fluid Mech.* **358**, 135–175.
OBLIGADO, M. & VASSILICOS, J.C. 2019 The non-equilibrium part of the inertial range in decaying homogeneous turbulence. *Europhys. Lett.* **127**, 64004.
OBOUKHOV, A.M. 1962 Some specific features of atmospheric turbulence. *J. Fluid Mech.* **13** (1), 77–81.
OBUKHOV, A.M. 1941 On the distribution of energy in the spectrum of turbulent flow. *Dokl. Akad. Nauk SSSR* **32**, 22–24.
PEARSON, B.R. & ANTONIA, R.A. 2001 Reynolds-number dependence of turbulent velocity and pressure increments. *J. Fluid Mech.* **444**, 343–382.
POPE, S.B. 2000 *Turbulent Flows*. Cambridge University Press.
QIAN, J. 1997 Inertial range and the finite Reynolds number effect of turbulence. *Phys. Rev.* E **55**, 337–342.
QIAN, J. 1999 Slow decay of the finite Reynolds number effect of turbulence. *Phys. Rev.* E **60**, 3409.
QIAN, J. 2000 Closure approach to high-order structure functions of turbulence. *Phys. Rev. Lett.* **84**, 646–649.
QIAN, J. 2001 Quasi-closure and scaling of turbulence. *Intl J. Mod. Phys.* B **15**, 1085–1116.
SADDOUGHI, S.G. & VEERAVALLI, S.V. 1994 Local isotropy of turbulent boundary layers at high Reynolds number. *J. Fluid Mech.* **268**, 333–372.
SAFFMAN, P.G. 1967 Note on the decay of homogeneous turbulence. *Phys. Fluids* **10**, 1349–1352.
SAGAUT, P. & CAMBON, C. 2018 *Homogeneous Turbulence Dynamics*. Springer.
SHE, Z.S. & LEVEQUE, E. 1994 Universal scaling laws in fully developed turbulence. *Phys. Rev. Lett.* **72** (3), 336.
SINHUBER, M., BEWLEY, G.P. & BODENSCHATZ, E. 2017 Dissipative effects on inertial-range statistics at high Reynolds numbers. *Phys. Rev. Lett.* **119** (13), 134502.

SINHUBER, M., BODENSCHATZ, E. & BEWLEY, G.P. 2015 Decay of turbulence at high Reynolds numbers. *Phys. Rev. Lett.* **114** (3), 034501.

SPEZIALE, C.G. & BERNARD, P.S. 1992 The energy decay in self-preserving isotropic turbulence revisited. *J. Fluid Mech.* **241**, 645–667.

SREENIVASAN, K. & ANTONIA, R.A. 1997 The phenomenology of small-scale turbulence. *Annu. Rev. Fluid Mech.* **29**, 435–472.

SREENIVASAN, K.R. 1984 On the scaling of the turbulence energy dissipation rate. *Phys. Fluids* **27**, 1048–1051.

STOLOVITZKY, G., SREENIVASAN, K.R. & JUNEJA, A. 1993 Scaling functions and scaling exponents in turbulence. *Phys. Rev.* E **48** (5), R3217–R3220.

TANG, S.L., ANTONIA, R.A., DJENIDI, L., DANAILA, L. & ZHOU, Y. 2017 Finite Reynolds number effect on the scaling range behavior of turbulent longitudinal velocity structure functions. *J. Fluid Mech.* **820**, 341–369.

TANG, S.L., ANTONIA, R.A., DJENIDI, L. & ZHOU, Y. 2020 Scaling of the turbulent energy dissipation correlation function. *J. Fluid Mech.* **891**, A26.

TCHOUFAG, J., SAGAUT, P. & CAMBON, C. 2012 Spectral approach to finite Reynolds number effects on Kolmogorov's 4/5 law in isotropic turbulence. *Phys. Fluids* **24** (1), 015107.

TOWNSEND, A.A. 1976 *The Structure of Turbulent Shear Flow*. Cambridge University Press.

TSUJI, Y. 2009 High-Reynolds-number experiments: the challenge of understanding universality in turbulence. *Fluid Dyn. Res.* **41**, 064003.

VASSILICOS, J.C. 2015 Dissipation in turbulent flows. *Annu. Rev. Fluid Mech.* **47**, 95–114.

WANG, L.-P., CHEN, S., BRASSEUR, J.G. & WYNGAARD, J.C. 1996 Examination of hypotheses in Kolmogorov refined turbulence theory through high-resolution simulations. Part 1. Velocity field. *J. Fluid Mech.* **309**, 113–156.

YEUNG, P.K. & BRASSEUR, J.G. 1991 The response of isotropic turbulence to isotropic and anisotropic forcing at the large scales. *Phys. Fluids* **3**, 884–897.

YEUNG, P.K. & ZHOU, Y. 1997 Universality of the Kolmogorov constant in numerical simulations of turbulence. *Phys. Rev.* E **56**, 1746–1752.

ZHOU, T. & ANTONIA, R.A. 2000 Reynolds number dependence of the small-scale structure of grid turbulence. *J. Fluid Mech.* **406**, 81–107.